The influence of electrostatic and -kinetic effects on droplet formation by a vibrating-mesh nebulizer

A.R. Speur

Delft University of Technology

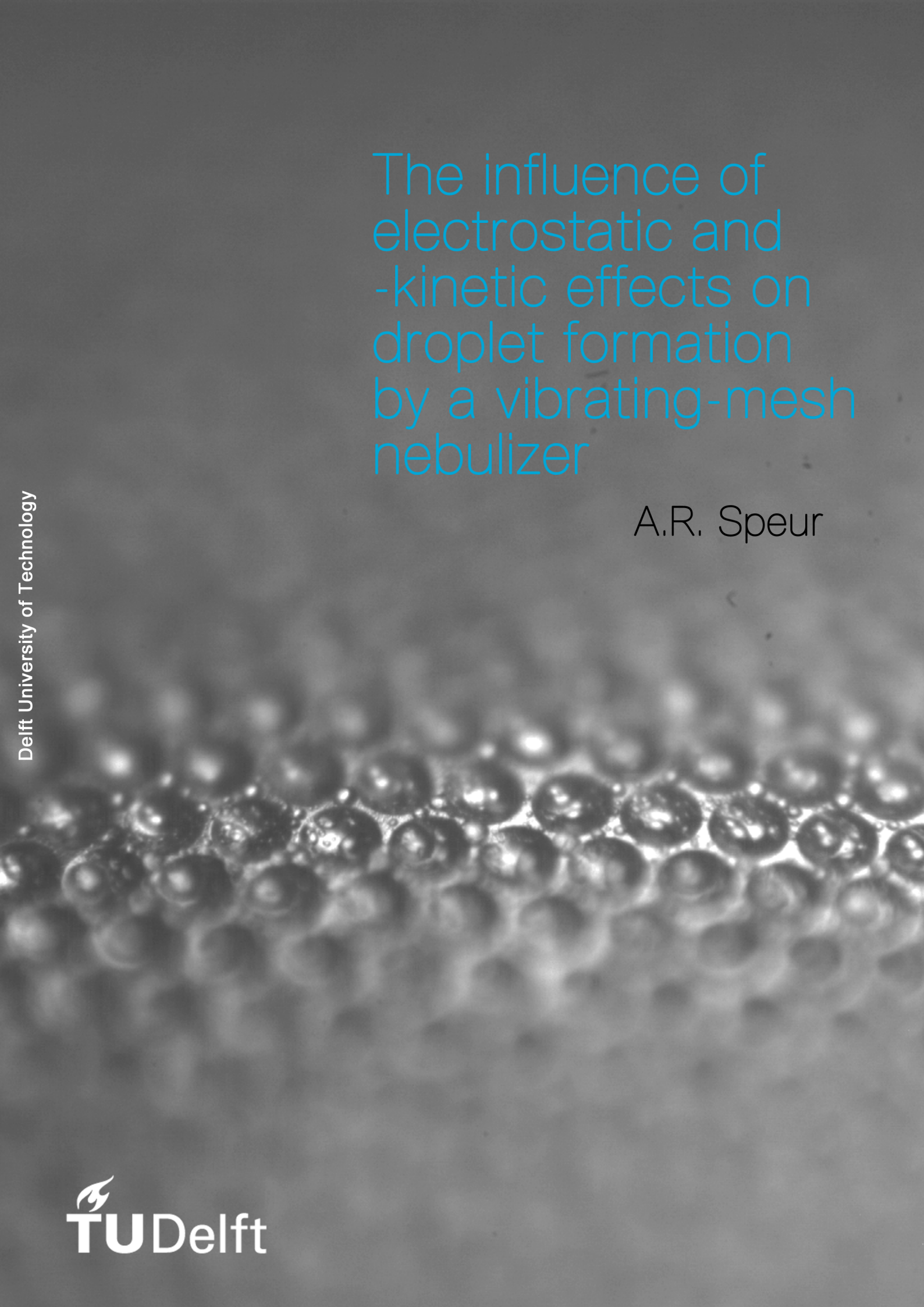

TU Delft

The influence of electrostatic and -kinetic effects on droplet formation by a vibrating-mesh nebulizer

by

A.R. Speur

4090047

to obtain the degree of Master of Science
at the Delft University of Technology,
to be defended publicly on October 4th 2018 at 02:00 PM.

Date:	17th September 2018
Daily supervisors:	Dr. H.B. Eral
	Dr.ir. W.P. Breugem
Thesis committee:	Prof.dr.ir. C. Poelma
	Dr. H.B. Eral
	Dr.ir. W.P. Breugem
	Ir. A. Verschueren

TU Delft Delft University of Technology

Preface

This thesis report has been written by A. R. Speur and tackles the investigation into the workings of a vibrating-mesh nebulizer. It is produced as a final product to obtain the degree of Master of Science at the Delft University of Technology. Anyone with an interest in the workings of the vibrating-mesh nebulizer or an interest in more fundamental mechanisms of droplet formation and electrostatics and -kinetics will enjoy reading this report.

I would like to thank my supervisors at the Delft University of Technology, Dr. H.B. Eral and Dr. ir. W.P. Breugem, for their excellent supervision and help during this project. I would like to thank Edwin, Bart, Michel and Jaap for helping me with all their expertise on the equipment I needed and lending me endless small and bigger parts for my set-up. I would like to thank Ir. A Verschueren from Philips for the opportunity to work on this interesting project and for providing me with as many nebulizers as I needed.

I would like to thank my parents and Georgia for helping me with the writing and rewriting of this report, and last but not least I would like to thank Ruby for all her kind encouragements, patience and support, it would not have been possible to do this without her.

Delft, 17th September 2018
A.R. Speur

Abstract

Using the respiratory system as a route to deliver medication has many advantages, such as the large surface area of the respiratory system and the ease of absorption via the lung tissue. Nebulizer technology uses the respiratory system to administer a wide variety of medication. Nebulizer technology creates microscale droplets that can be inhaled by the patient. Different types of nebulizer technology exists, and the vibrating-mesh nebulizer is one of them. A mesh with over a thousand nozzles, each with a diameter of 4.3 μm, vibrates against the liquid reservoir with a frequency of 128 kHz. This technology has already been proven to work, except for the use of one particular liquid, pure water.

The relation between the concentration of salt in a solution and the performance of the vibrating-mesh nebulizer was researched by Beck-Broichsitter et al. (2014). They found that a significant drop in performance takes place when the salt concentration of the solution decreases from 1 mM sodium-chloride to 0.01 mM sodium-chloride.

This research first investigated the theory on the properties of these solutions, and how these properties change when the concentration decreases from 1 mM sodium-chloride to 0.01 mM sodium-chloride. It was found that the hydrodynamic properties of the fluid do not change significantly over this range, but the electrostatic and -kinetic properties do change significantly over this range. This led to the hypothesis that the electrostatic and -kinetic effects have an influence on the formation of droplets and therefore the performance of the nebulizer. Three different hypotheses were contrived on how these effects influence the formation of droplets. The first hypothesis was that charged induced wetting causes the liquid from the nozzle to spread out over the surface at the end of the nozzle, instead of forming a droplet. The second hypothesis was that due to electrostatic forces in the neck of the droplet formation process, the neck is prevented to decrease in diameter, no pinch-off takes place and therefore no droplet is formed. The third hypothesis was that a droplet was formed, taking with it an electrostatic charge. The next droplet is then prevented from exiting the nozzle, by the electrostatic force the first droplet exerts on it. These hypotheses where based on engineering intuition, rather than experimental data.

Two different types of experiments were conducted to test the hypotheses. First the mass flow rate of the nebulizer was measured using different electrolyte solutions. Second, images where recorded, with various imaging speeds and magnifications, of the nebulizer while it was in working.

The results of the first type of experiments indicated that there is indeed a relation between the electrostatic and -kinetic properties of the fluid and the performance of the nebulizer. The results from the second type of experiments showed that the first hypothesis, the charged induced wetting hypothesis, was false. The results did not prove the other hypotheses to be false or true, but rather led to a new hypothesis. The new hypothesis was that the increased viscosity or decreased diameter of the nozzle, due to the electric double layer, bring down the mass flow through the nozzles or causes a portion of the nozzles to be inactive. As a prove of concept, an experiment was conducted where the viscosity of the liquid was decreased by increasing the temperature. This experiment gave the indication that the new hypothesis can be true.

Based on this research, it was recommended that the experimental set-up of the imaging experiments is improved by using a more advanced camera, by slowing down the droplet formation process, or by simplifying the nebulizer system. As a solution for the problem of not being able to nebulize pure water, an increase in temperature of the liquid or a coating of the mesh was recommended.

Contents

List of Symbols

η_0	Dynamic viscosity pure solvent	$\mathrm{Pa \cdot s}$
η	Dynamic viscosity	$\mathrm{Pa \cdot s}$
γ	Surface tension	$\mathrm{N \cdot m^{-1}}$
γ_0	Surface tension pure solvent	$\mathrm{N \cdot m^{-1}}$
γ_E	EulerMascheroni constant	$[-]$
κ	Debye-Hückel parameter	$\mathrm{mol^{-1/2} \cdot m^{3/2}}$
λ_B	Bjerrum length	m
Λ_{eq}	Molar equivalent conductivity	$\mathrm{S \cdot m^2 \cdot mol^{-1}}$
λ^0	Limiting equivalent conductance	$\mu\mathrm{S \cdot cm^{-1}}$
λ_D	Debye length	m
∇	Del operator	$\mathrm{m^{-1}}$
∇^*	Nondimensionalized del operator	$[-]$
ρ	Density	$\mathrm{kg \cdot m^3}$
σ	Electrical conductivity	$\mu\mathrm{S \cdot cm^{-1}}$
θ	Contact angle	rad
ε_0	Vacuum permittivity	$\mathrm{F \cdot m^{-1}}$
ε_r	Relative dielectric constant	$[-]$
ε	Relative permittivity	$\mathrm{F \cdot m}$
φ	Electric potential difference from bulk	$\mathrm{J \cdot C^{-1}}$
φ^*	Nondimensionalized electric potential difference from bulk	$[-]$
φ_0	Total potential drop across the double layer	$\mathrm{J \cdot C^{-1}}$
c	Concentration	$\mathrm{mmol \cdot L^{-1}}$
c_i	Concentration of ion i	$\mathrm{mmol \cdot L^{-1}}$
$c_{i,\infty}$	Concentration of ion i in bulk	$\mathrm{mmol \cdot L^{-1}}$
d	Tube diameter	m
e	Electron charge	C
e	Elementary charge	C
F	Faraday constant	$\mathrm{C \cdot mol^{-1}}$
I_c	Ionic strength	mM
k_B	Boltzmann constant	$\mathrm{J \cdot K^{-1}}$
L	Tube length	m
M_i	Molar mass of ion i	$\mathrm{g \cdot mol^{-1}}$

M_{H_2O}	Molar mass of water	$\mathrm{g \cdot mol^{-1}}$
N_A	Avogadro constant	$\mathrm{mol^{-1}}$
p	Pressure	Pa
p_b	Bernoulli pressure	Pa
p_c	Capillary pressure	Pa
p_i	Newton's second law pressure	Pa
p_v	Viscous pressure	Pa
R	Tube radius	m
R	Universal gas constant	$\mathrm{J \cdot mol^{-1} \cdot K^{-1}}$
r	Radial coordinate	m
T	Temperature	K
t	Time	s
u	Velocity	$\mathrm{m \cdot s^{-1}}$
V_i	Molar volume of ion i	$\mathrm{m^3 \cdot mol^{-1}}$
V_m	Molar volume	$\mathrm{m^3 \cdot mol^{-1}}$
V_{H_2O}	Molar volume of water	$\mathrm{m^3 \cdot mol^{-1}}$
We	Weber number	[−]
x	x coordinate	m
x_i	Molar fraction of ion i	[−]
x_{H_2O}	Molar fraction of water	[−]
y	y coordinate	m
z	z coordinate	m
z	Valence	[−]
z_i	Valence of ion i	[−]
${\Lambda^0}_{eq,+}$	Equivalent conductivity at infinite dilution of positive ion	$\mathrm{S \cdot m^2 \cdot mol^{-1}}$
${\Lambda^0}_{eq,-}$	Equivalent conductivity at infinite dilution of negative ion	$\mathrm{S \cdot m^2 \cdot mol^{-1}}$

Chapter 1

Introduction

Pulmonary drug delivery, using the lungs as a route to deliver medication into the bloodstream, is not necessarily a new science, but interest has increased with the possibility of using the lungs to deliver peptides and the achievability of gene therapy for Cystic Fibrosis (CF) (Jain, 2009). One of the advantages of pulmonary drug delivery is the large surface area of the respiratory system, which makes it very useful for absorption of oxygen, but also for the absorption of medication. A schematic of the respiratory system can be seen in Figure 1.1. For an adult, the surface area of the airways (the trachea, the bronchi and the bronchioles) is a few square metres, and the alveolar surface is more than 100 square metres (Patton and Byron, 2007). For the absorption of the medication, it is most effective to use methods of administration that ensure the medication finds its way into the alveolus.

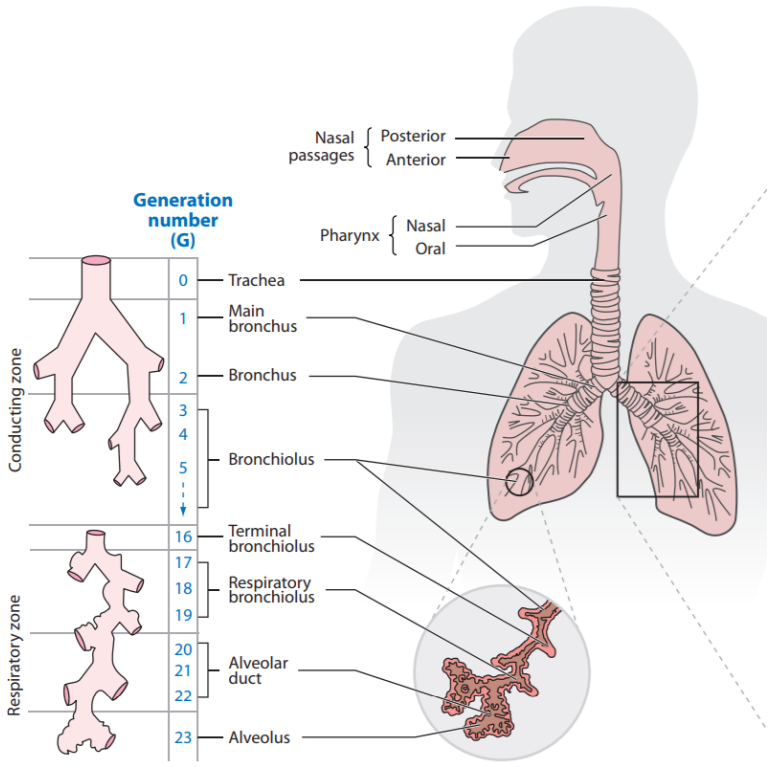

Figure 1.1: A schematic of the respiratory system. To have the highest possible absorption rate of medication via the respiratory system, the medication needs to reach the most intricate part of the system, the Alveolus. (Kleinstreuer and Zhang, 2010)

Inertia, gravity and diffusion can carry particles deep into the lungs, where the medication can be absorbed into the bloodstream of a patient (Muchão and da Silva Filho, 2010). This requires the size of these particles to be of a particular order of magnitude. In Figure 1.2 the ideal size of particles for different parts of the respiratory system can be seen. To reach the alveolus, it is therefore key that the particles are between 1 and 5 micrometer.

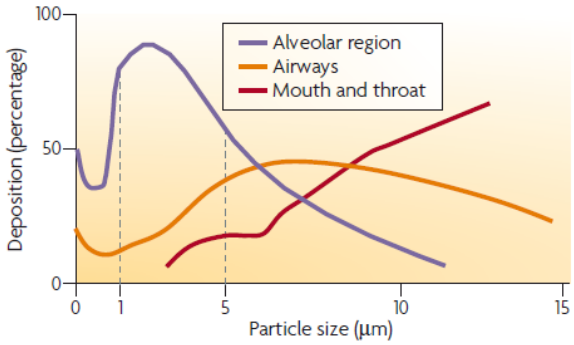

Figure 1.2: The deposition of particles of different sizes in different parts of the respiratory system (Patton and Byron, 2007).

Different methods exist for the delivery of particles into the respiratory system. Dry powder inhalers for asthma patients have been used for years (Patton and Byron, 2007). However, Philips uses a different type of system, a nebulizer. In contrast to the dry powder inhaler, this type of system is not limited to dry particles, but is able to deliver droplets of fluid into the lungs. A nebulizer makes droplets, so called aerosols, of a size specifically suitable for reaching the deepest parts of the lungs.

In the same way that there are different types of pulmonary drug delivery systems, there are also different types of nebulizers. Philips, and this report, are concerned with one particular type: the vibrating-mesh nebulizer. Figure 1.3 shows one of such devices. This device has been shown to work for many different types of fluids, except for a very particular one, pure water. Since the vibrating-mesh nebulizers have been shown to work for most intents and purposes, few have embarked on the journey to find the answer to the question: why is a vibrating-mesh nebulizer not capable of nebulizing pure water?

The intention of this research is to find the answer to this question, so that possible solutions for this problem can be proposed, and maybe even design changes can be made so that it will be possible to nebulize pure water, and the applications of the vibrating-mesh nebulizer can be extended.

Figure 1.3: The Aerogen Solo Nebulizer (Aer)

This report starts with the theory behind this device, what is known in literature about its performance, and the relevant theoretical background to fully understand the physical concepts this device relies

on. From the literature study, it is hypothesized what the possible reasons could be for the failure to nebulize pure water. From this hypothesis, experiments are designed to test this hypothesis. The way the experiments are conducted, the equipment that was used and the way data from the experiments was processed is described. The results of the experiments are displayed, together with a thorough explanation of the results, followed by a discussion on the interpretation of the results and its limitations. A conclusion is drawn from the results and the discussion. Does the hypothesis hold true? This question will be answered. Lastly, recommendations for improvement and further research are given.

Chapter 2

Theory

The Philips Nebulizer is an aerosol drug delivery system, traditionally meant for the delivery of medication for pulmonary diseases. The nebulizer creates aerosols, droplets with an average diameter of 5 μm, that can be inhaled by the patient.

2.1 Nebulizer technology

The nebulizer technology falls under the propellant driven metered dose inhalers, dry powder inhalers (Dalby and Suman, 2003). The advantages of the nebulizers are that high volumes of drugs and different types of drugs can be delivered to the patient, and it relies less on the patients correct use of the device than dry powder inhaler. Described here is the concept of nebulization, the different types of devices used for nebulization, with a more detailed description of the type of interest: the vibrating mesh nebulizer.

2.1.1 Concept of Nebulization

Nebulizer technology exists for the purpose of creating aerosols, which are suspensions of liquid droplets in a gas. If the droplet size of these aerosols are at a critical diameter of 1 to 5 μm, the aerosols can be delivered to the lungs of a patient. When the droplets are too small they will evaporate before reaching the desired destination, and when the droplets are too big they will collide with the airways before reaching the desired destination.

2.1.2 Different Types of Nebulizers

There are three different types of nebulizers, jet nebulizers, ultrasonic nebulizers and mesh nebulizers (Ari, 2014).

A jet nebulizer works with pressurized gas that flows through an orifice and then expands, causing a drop in pressure which forces the liquid from the reservoir to move towards this low pressure field and to break up into aerosols. An ultrasonic nebulizer works by means of a piezoelectric element that causes high frequency vibration in a liquid body, causing it to break up into aerosols at the liquid gas interface in the reservoir. A vibrating-mesh nebulizer has an oscillating mesh that causes a local high pressure on the reservoir side of the mesh, pushing liquid out on the other side, where it breaks up into droplets.

Each of these types has its own advantages and disadvantages. A jet nebulizer is effective for delivering substances that a dry powder inhaler cannot deliver, but has the disadvantages of needing compressed gas, increasing the complexity and having large amounts of residual fluid. Ultrasonic nebulizers have the same disadvantage of residual fluid, next to the inability to aerolize fluids with high viscosity. Mesh

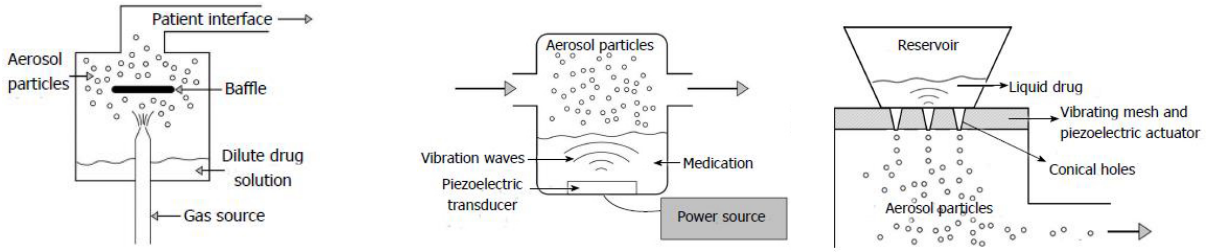

(a) A schematic of a jet nebulizer, where a gas flows through an orifice and then expands, causing a drop in pressure which forces the liquid from the reservoir to move towards this low pressure field and to break up into aerosols.

(b) A schematic of an ultrasonic nebulizer, where a piezoelectric element causes high frequency vibration in a liquid body, causing it to break up into aerosols at the liquid gas interface in the reservoir.

(c) A schematic of a vibrating-mesh nebulizer, where the oscillating mesh causes a local high pressure on the reservoir side of the mesh, pushing liquid out on the other side, where it breaks up into droplets.

Figure 2.1: Three different types of nebulizers (Muchão and da Silva Filho, 2010)

nebulizers have the advantage of not having large amount of residual fluids, and an increased output efficiency compared to jet and ultrasonic nebulizers (Ari, 2014).

A schematic view of a jet nebulizer can be found in Figure 2.1a, a schematic view of an ultrasonic nebulizer can be found in Figure 2.1b, and a schematic view of a vibrating-mesh nebulizer can be seen in Figure 2.1c.

2.1.3 Vibrating Mesh Nebulizer

This particular report is concerned with the vibrating-mesh nebulizer technology, and specifically the Aerogen solo vibrating mesh nebulizer. To have proper understanding of this device, a closer look is given into the literature about the working mechanism of the device and the geometry of the mesh. As can be seen in Figure 2.1c, aerosols are created by moving the mesh against a liquid surface, creating a local over pressure which pushes the liquid through the holes in the mesh. On the other side of these holes the liquid is pushed out of the holes and droplets are formed. A previous study done by (Chemmalasseri, 2012) on the working mechanism of the vibrating-mesh nebulizer resulted in a simulation in COMSOL that verified this working mechanism.

The mesh is vibrated by a piezoelectric actuator ring around the mesh, as can be seen in the top view in Figure 2.2. The piezoelectric crystal is actuated by an alternating voltage at a certain frequency, causing it to deform. This deformation of the piezoelectric crystal is translated into a deformation of the mesh, causing it to vibrate against the liquid surface in the reservoir.

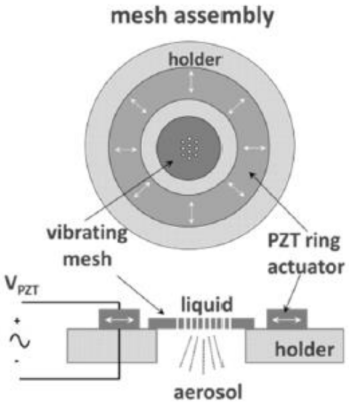

Figure 2.2: A schematic of the mesh assembly of a vibrating-mesh nebulizer. (Verschueren, 2017)

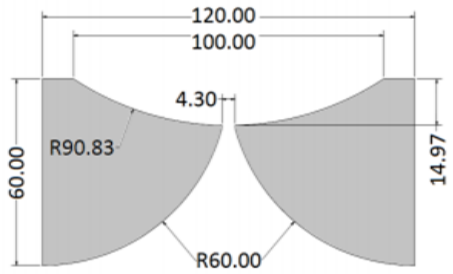

Figure 2.3: A schematic of a single nozzle in the mesh of a vibrating-mesh nebulizers , the dimensions are in μm (Verschueren, 2017)

The geometry of each of the holes in the mesh can be seen in Figure 2.3. When the nebulizer is working the liquid flows from bottom to top in the geometry in Figure 2.3. A more detailed investigation into the way the fluid flows through these holes and the formation of droplets when the liquid leaves the hole is provided in section 2.4.

To get an estimation of the mass flow rate of this particular model of vibrating-mesh nebulizer, a calculation was done to find this mass flow rate. Aer indicates that the mesh contains roughly 1000 nozzles, all of which are assumed to produce a single droplet every oscillation. It is assumed that the diameter of the droplet is on average the same size at the exit of the nozzle, so 4.3 μm in diameter. The density of water and the volume of a sphere with diameter 4.3 μm are used to determine the mass of a single droplet. The mass of a single droplet, the amount of oscillations per seconds given by the frequency of 128 kHz and the number of nozzle gives an indication that the mass flow rate of this model is around 0.32 gram per minute.

The mesh of the particular nebulizer discussed in this report is made of palladium, which is relevant for the interaction between the solid material of the mesh and the liquid that passes through the mesh. An in-depth description of this interaction is discussed in section 2.4.

2.2 Nebulizer performance

Previous studies by Beck-Broichsitter et al. (2014) and Ghazanfari et al. (2007) have shown there is a relationship between the performance, indicated by the output rate, and molarity of an electrolyte solution, used to nebulize. As can be seen in Figure 2.4, when going to extremely low concentrations of salt, the output rate of the vibrating mesh nebulizer decreases significantly.

The output rate of the nebulizer depends on the physiochemical properties of the fluid to be nebulized. Several studies show dependencies between the output rate of the vibrating mesh nebulizer and different properties. Each of these properties and their influence on the output rate are discussed here, divided into the hydrodynamic properties and electrostatic and -kinetic properties. For each property there is looked at the change of the property over the range of concentration where the output range varies significantly. This range where the output rate varies significantly is derived from Figure 2.4 and goes from 0.01 mM to 0.1 mM.

Since the figure used as a reference for this research project, revolves around a sodium-chloride solution, this solution is the fluid used in the following determination of physiochemical properties.

The exact computation of the change in both the hydrodynamic en electrostatic and -kinetic properties can be found in detail in Appendix A. In the sections below, for readability, only the model used and

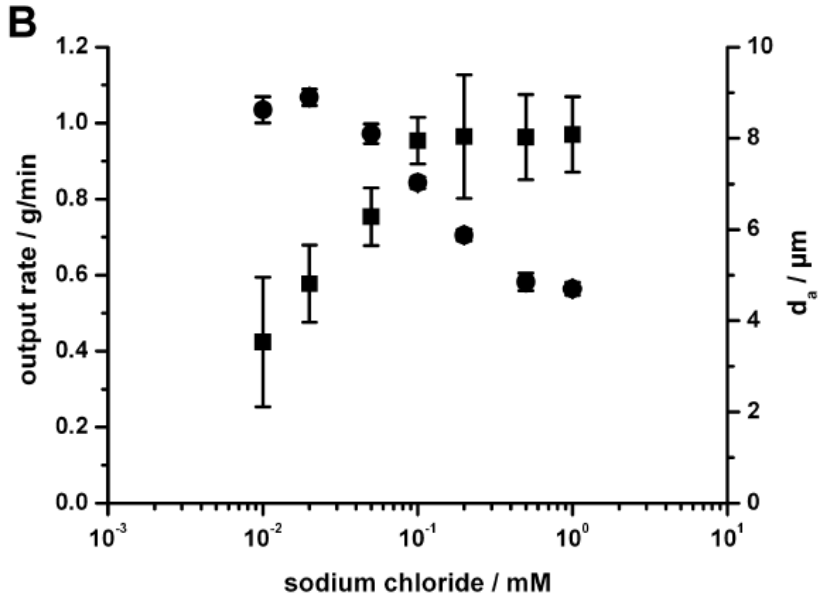

Figure 2.4: The output rate of a vibrating-mesh nebulizer, where the square data points are the output rate for a given molarity of a sodium-chloride solution, and the diamond shaped data points are the average aerodynamic diameter of the aerosols produced for a given molarity of a sodium-chloride solution (Beck-Broichsitter et al., 2014).

the resulting change of each of the properties is discussed.

2.2.1 Hydrodynamic properties

Naturally, when treating the formation of droplets, classical fluid mechanics comes to mind. Each important property of a fluid from that perspective is treated here, and the relation between each property and the output rate is discussed.

Viscosity

The viscosity changes when the concentration of added electrolytes changes. Over time, several different models describing the relationship between the electrolyte concentration and the viscosity have been proposed (Jiang and Sandler, 2003).

In early 1900, Grüneisen found, through experiments at very low concentrations, that there is a non-linear relationship between the viscosity of an electrolyte solution and the concentration (Jiang and Sandler, 2003). The relationship can be found in Equation 2.1 and is valid for concentrations lower than 0.01 M, which fits well with the above discussed range.

$$\eta/\eta_0 = 1 + A\sqrt{c} \tag{2.1}$$

Here, η and η_0 represent the viscosity of the solution and the viscosity of the solvent respectively, and c is the concentration of electrolytes in the solution. The positive constant A in Equation 2.1 can be determined using Equation 2.2 (Patil et al., 2014). The limiting equivalent conductance's λ_1^0 and λ_2^0 are properties of the selected ions for the electrolyte solution, in this case sodium and chloride (Miller et al., 1988).

$$A = 0.7536 \left[\frac{\lambda_1^0 + \lambda_2^0}{4\lambda_1^0\lambda_2^0} - \frac{\left(\lambda_1^0 - \lambda_2^0\right)^2}{4.41\lambda_1^0\lambda_2^0\left(\lambda_1^0 + \lambda_1^0\right)} \right] \tag{2.2}$$

The limiting equivalent conductance's λ_1^0 and λ_2^0 are properties of the selected ions for the electrolyte solution, in this case sodium and chloride (Miller et al., 1988).

Using these equations to determine the change in viscosity over the given range of concentrations, it is found the viscosity changes less than 1 percent over this range. The magnitudes of the relevant parameters and the exact computation of the change in viscosity can be found in Appendix A.

Increasing the viscosity has shown to lead to a decreasing output rate (Beck-Broichsitter et al., 2014). However, the very small change in viscosity found above for the range of concentration sodium-chloride, is not significant enough to explain the change in output rate over this range (Ghazanfari et al., 2007).

Surface tension

There is an excess surface tension for an electrolyte solution compared to its pure solvent. For this excess surface tension an analytic expressions exists (Ohshima and Matsubara, 2004):

$$\gamma = \gamma_0 + \frac{1}{2} z^2 \lambda_B c k_B T \left[\ln\left(\frac{2}{\kappa \lambda_B}\right) - 2\gamma_E + \frac{3}{2} \right] \tag{2.3}$$

where γ and γ_0 are the surface tension of the solution and the solvent, z is the valence of the ions in the solution, k_B is the Boltzmann constant given by $k_B = 1.38064852 \cdot 10^{-23}\ m^2\ \mathrm{kg}/s^2/\mathrm{K}$, T is the temperature of the solution, γ_E is the Euler-Mascheroni constant given by $\gamma_E = 0.57722$, κ is the Debye-Hückel parameter given by:

$$\kappa = \sqrt{\frac{2cz^2e}{\varepsilon_0 \varepsilon_r k_B T}} \tag{2.4}$$

where e is the elementary charge given by $e = 1.602177 \cdot 10^{-19}$ C, ε_0 is the vacuum permittivity given by $\varepsilon_0 = 8.854188 \cdot 10^{-12}$ F/m and ε_r is the relative dielectric constant of the solvent.

Finally, in Equation 2.3, λ_B is the Bjerrum length, defined as:

$$\lambda_B = \frac{e^2}{4\pi \varepsilon_0 \varepsilon_r k_B T} \tag{2.5}$$

Using this equation to determine the change in surface tension between the 0.01 mM and 0.1 mM solutions, it is found the surface tension changes far less than 1 percent over this range. The magnitudes of the relevant parameters and the exact computation of the change in surface tension can be found in Appendix A.

Decreasing the surface tension has been shown to increase the output rate when the viscosity of the fluid is low (Ghazanfari et al., 2007). This would mean the increase in output rate for higher concentration is counteracted by the increase in surface tension. However, the change in surface tension is so small it can be assumed to have negligible influence on the output rate.

Contact Angle

For a flat rigid surface the contact angle, the angle where the liquid-gas interface meets the solid surface, can be determined using Young's equation as seen in Equation 2.6 (Good, 1992).

$$\cos(\theta) = \frac{\gamma_{SG} - \gamma_{SL}}{\gamma_{LG}} \tag{2.6}$$

Here, θ is the contact angle, γ is the surface tension where the subscripts denote the surface tension between different phases: solid, liquid and gas.

Previously it was determined the surface tension does not change significantly over the range discussed. It is therefore assumed the same holds for the contact angle, since it is directly related to the surface tension.

Density

The density changes when the concentration of an electrolyte solution changes. The change in density can be described by (Li and Lee, 1998):

$$\rho = \frac{\sum_{i=1}^{ion} x_i M_i + x_{H_2O} M_{H_2O}}{V_m} \tag{2.7}$$

where ρ is the density of the solution, x_i is the molar fraction of the species i in the solution, M_i is the molar mass of species i, x_{H_2O} is the molar fraction of water in the solution, M_{H_2O} is the molar mass of water in the solution and V_m is the molar volume, which can be determined using:

$$V_m = \sum_{i}^{ion} x_i V_i + x_{H_2O} V_{H_2O}^{\Phi} \tag{2.8}$$

where V_i is the molar volume of species i and V_{H_2O} is the molar volume of water.

Using this model to compute the density over the range of concentrations, it is found the density varies less than 1 percent. The magnitudes of the relevant parameters and the exact computation of the change in density can be found in Appendix A.

Thus far, no definitive relation has been determined between the density of the fluid and the output rate (Carvalho and McConville, 2016). The insignificant change of density over the concentration range does not indicate the possible existence of such a relationship for this range of concentrations.

2.2.2 Electrostatic and -kinetic properties

Until now, no strong relation between the discussed properties of the fluid and the output rate of the nebulizer was found for the solution range at which the nebulizer has a significant increase in performance. This suggests these properties do not have a large enough influence on the formation of droplets at these small concentrations, and other properties need to be taken into account. Moving away from the hydrodynamic properties and looking into the electrostatic and -kinetic properties, the electrical conductivity of the fluid shows other results.

Electrical conductivity

A strong relationship exists between the conductivity of a fluid and the concentration of electrolytes in the fluid. The conductivity of an electrolyte solution can be determined using (Kirby, 2013):

$$\sigma = c\Lambda_{eq} \tag{2.9}$$

where σ is the conductivity of the solution and λ_{eq} is the molar equivalent conductivity of the solution. This molar equivalent conductivity can be determined with (Atkins, 1892):

$$\Lambda_{eq} = ({\Lambda^0}_{eq,+} + {\Lambda^0}_{eq,-}) - \left(\frac{z^3 e^3 N_A}{3\pi\eta} \sqrt{\frac{2N_A}{\varepsilon k_B T}} + ({\Lambda^0}_{eq,+} + {\Lambda^0}_{eq,-}) \frac{z^3 e^3}{24\pi\varepsilon k_B T \left(1 + \sqrt{\frac{1}{2}}\right)} \sqrt{\frac{2N_A}{\varepsilon k_B T}} \right) \sqrt{c} \tag{2.10}$$

where ${\Lambda^0}_{eq,-}$ and ${\Lambda^0}_{eq,+}$ are the equivalent conductivities at infinite dilution of the negative and positive ions in the solution, N_A is Avogadro's constant, given by $N_A = 6.022 \cdot 10^{23}\ mol^{-1}$ and ε is the relative permittivity of the solvent.

Computing the electrical conductivity for the sodium-chloride solution over the relevant range gives a strong increase in the conductivity of the liquid. The magnitudes of the relevant parameters and the exact computation of the increase in electrical conductivity can be found in Appendix A.

The hypothesis exists that an increase in electrolyte present increases the conductivity and suppresses the electrostatic charge present in pure water, therefore increasing the output rate of the nebulizer (Beck-Broichsitter et al., 2014). It was recommended further research is conducted on this hypothesis (Ghazanfari et al., 2007).

2.3 Problem description

The output rate of the nebulizer varies significantly over a small range of electrolyte concentrations, illustrated in Figure 2.4. As discussed in section 2.2, several properties of the flow investigated for their influence on the performance of the nebulizer, but the literature showed no definitive answer as to what the reason is for this sudden drop in output rate when going to low concentrations of electrolytes.

Looking at the negligible changes in hydrodynamic properties such as the surface tension or the viscosity, these properties appear not to be the cause in the drop-off in output rate at low concentration.

In recent literature, it has been suggested that the electrostatic and -kinetic properties of the fluid may play a role in the output rate, since changes in these properties are much larger than the changes in hydrodynamic properties. The study by Ghazanfari et al. (2007) suggests that this may be a direction where the answer lies.

Therefore, the main questions that arise are, if the hydrodynamic properties do not influence the output rate at low electrolyte concentrations, what other mechanisms are at play? Is the drop-off in output rate related to the electrostatic and -kinetic properties of the fluid? What mechanisms are influenced by the electrostatic and -kinetic properties and how do these mechanisms disturb the formation of droplets when nebulizing?

2.4 Theoretical background

To understand the physics behind the problem, a deeper look into the theory of different aspects is needed. Again, in the same way as in section 2.2, the theory is divided into classical fluid mechanics and electrostatic and -kinetic theory.

2.4.1 Fluid mechanics

Investigation into the fluid mechanics of this problem starts with the driving mechanism of the flow through the holes in the mesh. This driving mechanism leads to an understanding of the state of the flow when it leaves the mesh to form droplets. Following this, the process of droplet formation at the exit of the holes in the mesh is described.

Pressure driven flow

The movement of the mesh creates an oscillating pressure in the fluid close to the mesh, causing the fluid to be pushed through the nozzles in the mesh when the pressure is at its highest. The magnitude of the pressure difference required to form droplets can be deduced from the forces that counteract the movement of flow through the holes and the forces needed for the formation of a droplet at the end of the tube.

According to Wijshoff (2010), to generate a drop at the end of the nozzle, the pressure at the entrance of the nozzle has to be high enough to overcome inertia of the liquid, both steady and unsteady, the viscous forces acting on the liquid inside the nozzle and the forces by the surface tension at the liquid-gas interface at the end of the nozzle. Each of these pressure forces can be determined as follows.

The pressure required to overcome steady inertia is given by the Bernoulli pressure:

$$p_b = \frac{1}{2}\rho {u_\omega}^2 \tag{2.11}$$

where ρ is the density of water, and u_ω is the maximum velocity of the liquid inside the nozzle, which can be determined according to Chemmalasseri (2012) as:

$$u_\omega = \omega \cdot R \tag{2.12}$$

where ω is the angular frequency, which can be determined by multiplying the frequency of oscillation with 2π. The frequency of oscillation, as mentioned before, is 128 kHz. Filling in the properties gives a Bernoulli pressure of 0.0149 bar.

The unsteady pressure follows from Newton's second law and is determined by:

$$p_i = \rho L \frac{du}{dt} \tag{2.13}$$

where L is the length of the nozzle. Since the nozzle has a strong curvature, and Equation 2.13 assumes a rectangular channel (Wijshoff, 2010), an estimation needs to be made for the approximated length of the rectangular equivalent of the nozzle. Looking at Figure 2.3, it is assumed that the length of the nozzle is of the order of magnitude as the diameter of the nozzle, so 4.3 μm. It is assumed that the acceleration of the liquid can be determined as follows (Chemmalasseri, 2012):

$$\frac{du}{dt} = u_\omega \cdot \omega \tag{2.14}$$

Computing the unsteady inertial pressure then gives p_i=0.0597 bar.

To find the viscous forces on the liquid, it is assumed that the flow in the nozzle acts as a Poiseuille flow, which means the viscous pressure can be determined using:

$$p_v = \frac{8\eta L u_\omega}{R^2} \tag{2.15}$$

Using the same parameters as described above gives a viscous pressure of 0.1289 bar.

Lastly the pressure by the surface tension can be determined using:

$$p_c = \frac{2\gamma \cos(\theta)}{R} \tag{2.16}$$

where it can be assumed that $cos(\theta)$=1 due to the sharp edge of the nozzle orifice (Chemmalasseri, 2012), which leads to a pressure due to the surface tension of 0.6698 bar.

According to Chemmalasseri (2012), adding up the above determined pressures gives a total pressure best represented by the root-mean-squared value of the pressure, due to the sinusoidal nature of the pressure signal, the maximum pressure can then be determined by:

$$p_{\max} = p_{RMS} \cdot \sqrt{2} = (p_b + p_i + p_v + p_c) \cdot \sqrt{2} \tag{2.17}$$

The maximum amplitude of the oscillating pressure signal is then determined as 1.2350 bar.

The geometry of each of the holes in the mesh is approximated as a tube through the mesh, as can be found in Figure 2.3. The geometry is assumed to be axisymetric along the length of the tube. To analytically describe the flow through the geometry, a few assumptions were to be made.

A first assumption is made that the flow through the tube behaves as a unidirectional flow. This greatly simplifies the Navier-Stokes equations. The second assumption that is made, is that due to the very small dimensions of the tube, the flow is laminar. Since it is known through the workings of the nebulizer that the flow is pressure induced, the flow through the tube can be approximated by the Hagen-Poiseuille solution for pressure-driven laminar flow (Kirby, 2013).

The Hagen-Poiseuille equation, derived from the Navier-Stokes equation using the above mentioned assumptions, gives the velocity profile over the radius of the tube as presented in Equation 2.18 (Kundu et al., 2016), where the driving pressure was previously determined. The resulting velocity profile is presented in a cylindrical coordinate system with the z-axis parallel to the walls of the tube and the radial axis perpendicular to the z-axis. A detailed derivation of the Hagen-Poiseuille equation starting at the Navier-Stokes equation can be found in Appendix A.

$$u_z = -\frac{1}{4\eta}\frac{\partial p}{\partial z}\left(R^2 - r^2\right) \tag{2.18}$$

Droplet formation

To understand why droplets will or will not form it is important to have a closer look at the dynamics of droplet formation. To have more insight at the mode of droplet formation, the Weber number can be computed as found in Equation 2.19 (Oliemans, 2011).

$$We = \frac{\rho {u_\omega}^2 D}{\gamma} \tag{2.19}$$

where D is the diameter of the nozzle. The Weber number represents the ratio between inertial forces and surface tension forces. When the Weber number is small, so when the surface tension forces are large compared to the inertial forces, droplets form right at the entrance of the tube, so called dripping. When the Weber number is large, so when the inertial forces are large compared to the surface tension forces, the fluid leaves the tube as a jet, which further downstream breaks up into droplets. Considering the previously mentioned parameters, it is found that for this particular case the Weber number is equal to 0.0891. This indicates that this case acts in the dripping regime, meaning droplets form right after the liquid is ejected from the tube, as illustrated in Figure 2.5.

To estimate the influence of gravity on the droplet formation process, the Ëotvös number can be computed. This number is determined by the ratio of gravitational forces and surface tension forces and is given by (Oliemans, 2011):

$$Eo = \frac{\rho g D^2}{\gamma} \tag{2.20}$$

Computing the Ëotvös gives that it is equal to $2.51{\cdot}10^{-6}$, so extremely small. This indicates that for this particular case, gravity does not play a large role in the formation of droplets.

To estimate the influence of gravity on the droplet after it is formed and is moving away from the mesh, the Froude number can be computed. This number represents the ratio of the inertia of the droplet and gravitational forces on the droplet. The Froude number is given by (Oliemans, 2011):

$$Fr = \frac{u}{\sqrt{gD}} \tag{2.21}$$

Computing the Froude number gives that is equal to $2.84{\cdot}10^{5}$, indicating that the droplet has a high enough inertia to not be influenced in its trajectory by gravity. However, if the droplet is slowed down

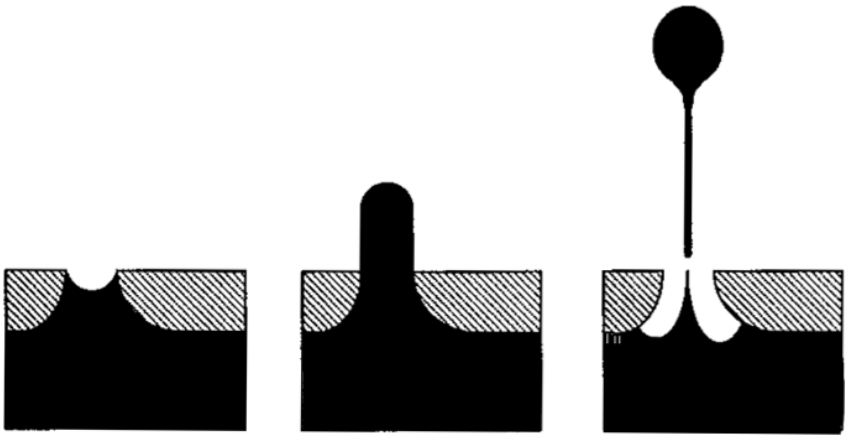

Figure 2.5: An illustration of the formation of droplets, adapted from Le (1999). In the article by Le (1999) the process of droplet formation for inkjet printing is described. In that process, the driving force for the liquid to be pushed through the nozzle is a pressure on the liquid created by a gas bubble in the reservoir. In the vibrating-mesh nebulizer this pressure on the liquid is created by a different process, the oscillation of the mesh. The effect however, is similar: a pressure driven flow through the nozzle.

sufficiently, for example by drag on the droplet, the Froude number drops and the droplet may become susceptible to gravitational forces.

The lack of influence of gravity on the droplet will prevent it from taking on a trajectory (partly) in the direction of gravity, but is not a prediction of the shape of its trajectory. To determine the trajectory of a droplet, the density ratio of the fluid of the droplet and the surrounding gas is required, together with the Galilei number (Jenny et al., 2013). The Galilei number is determined by:

$$Ga = \frac{\rho g D^3}{\eta^2} \tag{2.22}$$

where ρ and η are the density and viscosity of the droplet. Computing the Galilei number gives that it is equal to $7.76{\cdot}10^{-7}$. Since the density ratio is much larger than one, this leads to the conclusion that the droplet will move in a straight trajectory when it leaves the mesh (Jenny et al., 2013).

The formation of the droplet can be described by the breakup of a thin liquid jet (Drazin, 2002). At the exit of the tube an instability causes a neck to appear. The surface tension of the liquid-gas interface at this neck causes an increase in pressure at the neck. The pressure in this neck, due to surface tension forces, becomes higher than the pressure in the liquid next to the neck, causing a flow of the liquid from the neck towards the bulk of the fluid, the droplet. The neck decreases in diameter due to this outflow, until it no longer exists, a pinch off of the droplet occurs.

2.4.2 Electrostatics and -kinetics

Now that the mechanisms that drive the flow through the mesh and that form the droplet are clear, a closer look is taken into the electrostatic and -kinetic effects that take place on the small scale of this particular problem.

At a macro scale, the fluid-solid interaction is determined by well know fluid mechanics boundary conditions such as no slip at the wall and no penetration of the wall. At a micro scale however, different effect take place at this boundary, that are not taken into account in classical fluid mechanics. The scale of this problem is that of the micro scale, since the diameter of a single nozzle is 4.3 μm. This leads to the requirement of a further investigation into the electrostatic and -kinetic effect.

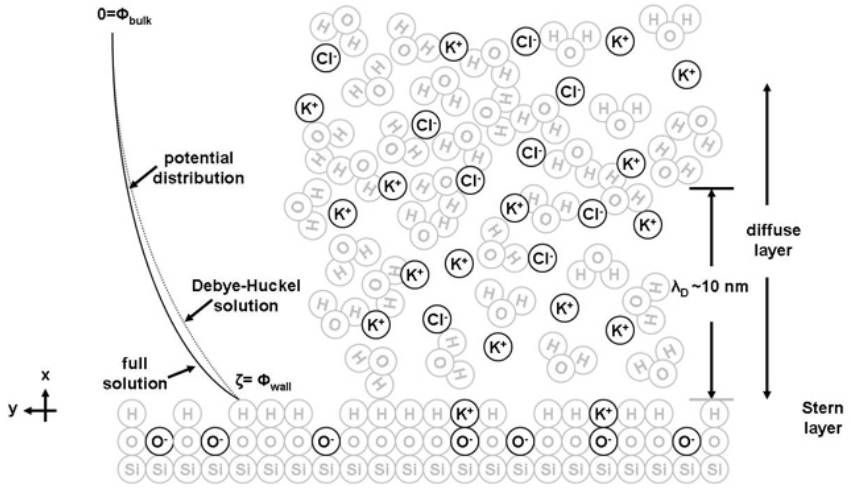

Figure 2.6: A solid silicon surface attracts negative ions from a potassium-chloride solution, creating a layer of negative charged ions called the Stern layer. As a reaction to this negatively charged Stern layer, positive ions form a diffuse layer in the liquid close to the silicon surface with a characteristic length often referred to as the Debye length (Kirby, 2013).

Electric double layer

Starting at the solid, different kinds of processes, such as ionization and absorption processes, lead to a nonzero surface charge density at the surface of a solid interacting with an aqueous solution, also known as the Stern layer (Kirby, 2013). This surface charge leads to a potential difference between the solid-liquid interface and the bulk of the solution. Close to the surface of the solid an accumulation of opposite charged ions counteract the charge of the solid, this accumulation is called the electric double layer (Stojek, 2005). This layer is, unlike the bulk of the solution, not electroneutral, so the net charge density in this layer is not zero. The concentration of opposite charged ions diffuses into the bulk, causing this electric double layer to be of a finite thickness, this characteristic thickness is often referred to as the Debye length (Kirby, 2013). An illustration of a metal surface, the Stern layer and the diffuse layer of ions can be found in Figure 2.6. The Debye length and its computation are discussed in more detail in the section below.

Surface charge of the solid

As mentioned the solid material in contact with an aqueous solution has a nonzero surface charge. This surface charge is determined by the pH of the aqueous solution (when concerned with water) and is governed by the adsorption of ions from the solution (Kosmulski, 2011). At a certain pH of the solution the surface adsorpts such an amount of ions from the solution that there is no surface charge. This pH is called the point of zero charge (pzc), and is a property of the solid material. When the pH of a solution is below the pzc of the material, the solid adsorpts more hydrons than hydroxide groups and the surface is positively charged, attracting anions. When the pH of the solution is higher than the pzc, the solid adsorpts more hydroxide groups than hydrons and the surface is negatively charged, attracting cations.

Since the pzc is a property specific to the material, the pzc of palladium can be determined. According to Le et al. (2017) the pzc of palladium is 5.25. Solutions with a pH higher that 5.25 will therefore lead to a negative surface charge, while solutions with a pH lower than 5.25 will lead to a positive surface charge.

Potential in the fluid

Now that it is clear what happens at the solid surface, the effect of this in the liquid can be described. The dissipation of charge in the liquid close to the solid surface can be represented by the link between the ion distribution (or local net charge density) in the liquid and the change in potential between the solid

liquid interface and the bulk fluid. This relation can be represented by the Poisson-Boltzmann equation, when looking at it s a quasi 1-D analysis in a semi-infinite domain (Kirby, 2013). The Poisson-Boltzmann equation is then:

$$\nabla^2\varphi = -\frac{1}{\varepsilon}\sum_i c_{i,\infty}\exp\left[\frac{-z_iF\varphi}{RT}\right]z_iF \tag{2.23}$$

Here φ is the electric potential difference from the bulk of the fluid, $c_{i,\infty}$ is the concentration of species i in the bulk of the fluid, F is the Faraday constant and is equal to F = 96485.3329 C·mol^{-1}, and z_i is the valence of species i.

This differential equation can be non-dimensionalised, starting with normalising the potential with the thermal voltage as seen in Equation 2.24.

$$\varphi^* = \frac{\varphi}{RT/F} \tag{2.24}$$

The second derivative with respect to length can be normalised with the Debye length squared as illustrated in Equation 2.25.

$$\nabla^{*2} = {\lambda_D}^2\nabla^2 \tag{2.25}$$

The Debye length is defined in Equation 2.26 and is always evaluated in the bulk of the fluid. The Debye length can be considered as the distance over which the ions of opposite charge to the solid surface dissipate from a high concentration close to the wall to a low concentration in the bulk of the fluid. The ionic strength used to determine the Debye length is defined in Equation 2.27. The Debye length is strongly dependent on the ionic strength of the solution, which in its turn depends on both the concentration of the electrolytes and its valance. This leads to a difference of Debye lengths between solutions of an order of magnitude. To be more specific, the Debye length of DI water is 980 nm, whereas the Debye length of a 1 mM sodium-chloride solution is 13.6 nm. The diameter of a single nozzle is 4.3 μmeter, so only around 4.4 times the Debye length of DI water, but around 320 times the Debye length of a 1 mM sodium-chloride solution. This illustrates the significance of this characteristic length for this particular problem.

$$\lambda_D = \sqrt{\frac{\varepsilon RT}{2F^2I_c}} \tag{2.26}$$

$$I_c = \sum_i c_i{z_i}^2 \tag{2.27}$$

Filling in the normalised parameters this leads to the non-dimensionalised Poisson-Boltzman equation as shown in Equation 2.28.

$$\nabla^{*2}\varphi^2 = -\frac{1}{2}\sum_i {c_{i,\infty}}^* z_i\exp\left[-z_i\varphi^*\right] \tag{2.28}$$

No general solution exists for this differential equation. However, by assuming a symmetric electrolyte, a long circular tube and a thick electric double layer, so when the Debye length is of the order of magnitude of the radius of the tube, a solution can be derived as shown in Equation 2.29 (Kirby, 2013).

$$\frac{\varphi}{\varphi_0} = \frac{\cosh\left(y/\lambda_D\right)}{\cosh\left(d/\lambda_D\right)} \tag{2.29}$$

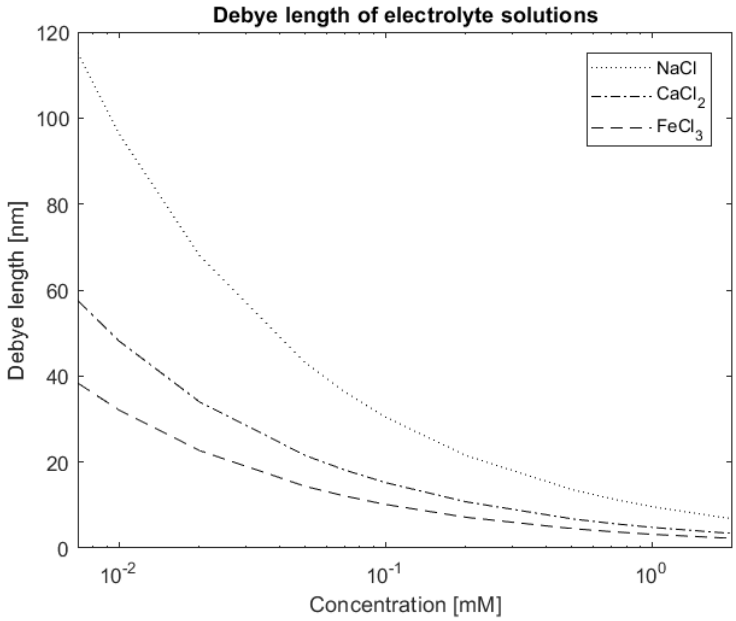

Figure 2.7: The Debye length for three different electrolyte solutions at different concentrations of electrolytes.

This equation shows that the Debye length is the relevant length scale that characterises the solution. The ratio between the tube diameter and the Debye length can vary greatly over a small range of concentrations or for electrolytes with different valences. To get a sense of the magnitude of the Debye length for these different solutions, a range of them is plotted in Figure 2.7

To give an indication of the influence of the potential on the flow on the micro scale this problem concerns, the normalised potential of different electrolyte solutions over the tube radius is plotted together with the velocity profile over the tube radius in Figure 2.8.

2.5 Hypothesis

Based on the theory describing the physical phenomena concerned with the formation of droplets by the vibrating mesh nebulizer, a hypothesis can be made about the answers to the questions that arose in section 2.2 and section 2.3.

It is hypothesised that the electrostatic and -kinetic effects do have an influence on the formation of droplets and therefore the mass flow rate of the nebulizer. Theory shows that a diffusive layer of positive ions forms in the small nozzles of the mesh. By moving the fluid out of the nozzle by the induced pressure difference, this layer will move along with the flow. By increasing the concentration of the electrolyte solution, or using a different electrolyte with a higher valence, theory predicts this diffusive layer of positive ions will become smaller. Due to the expected parabolic velocity profile in the channel, with a smaller layer, the positive ions will move at a lower velocity.

The hypothesis on how this diffusive layer of positive ions influences the formation of droplets consists of three different possibilities. The first hypothesis on the failure of droplet formation is that charge induced wetting takes place. The electric charge in the liquid changes the wettability properties of the liquid. So when the liquid is expelled from the channel, it then forms a liquid layer on top of the mesh instead of forming a droplet.

The second hypothesis on the failure of droplet formation is the stabilisation of the neck during the process of droplet formation. As described in section 2.4, the neck of the liquid column expelled from the holes decreases due to the pressure induced by the surface tension force of the liquid-gas interface. It

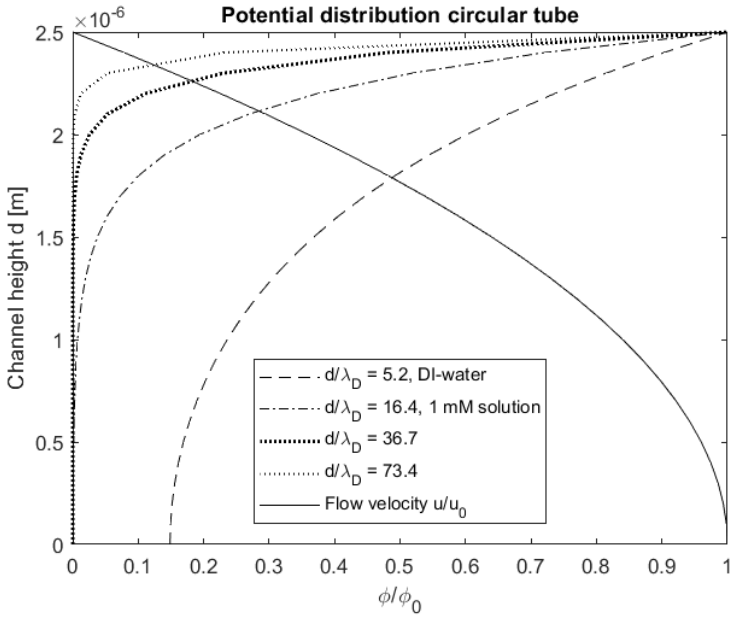

Figure 2.8: A plot of different electrolyte solutions, where the concentration and valence of the different solutions lead to different ratios of the Debye length and tube diameter. The channel height represents the radius of the tube, so only half of the channels diameter, where the origin of the y-axis represents the middle of the channel. Since the solution is symmetric, it can be mirrored over the x-axis to find the solution for the entire channel diameter.

is hypothesised that when the neck has grown significantly small, the diffusive layers of positive ions will be in such close proximity that the electrostatic repulsion of these positive charges will be large enough to withstand the surface tension force. Due to this balance, the radius of the neck will not go to zero, so no pinch off takes place. It is unlikely that the fluid will form a continuous jet when no pinch off takes place. The small scale of the problem causes the inertia of the liquid to be quite small. It is therefore more likely that the liquid will pushed back into the nozzle by the forces caused by surface tension.

The third hypothesis is a droplet is formed, taking with it the positive charge of the diffusive layer. Since the droplets are formed periodically, the next droplet will form behind this positively charged droplet. It is hypothesised the electrostatic repulsion of both droplets will be large enough for the second droplet to be pushed back into the hole instead of following the first droplet away from the mesh.

An schematic overview of the three hypothesis can be found in Figure 2.9 - Figure 2.11. Figure 2.9 represents the first hypothesis of charged induced wetting. Figure 2.10 represents the hypothesis of no pinch off, and Figure 2.11 represents the hypothesis of electrostatic repulsion.

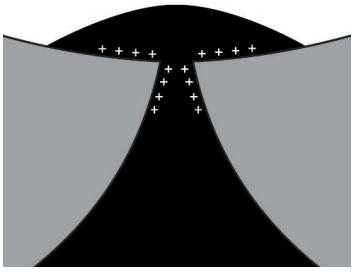

Figure 2.9: The hypothesis that the nebulizer fails to nebulize a aqueous solution due to electrowetting effects causing the liquid to form a liquid pool on the surface of the mesh instead of forming a droplet.

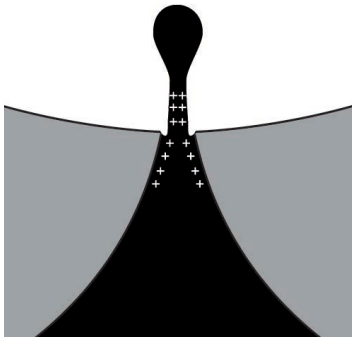

Figure 2.10: The hypothesis that the nebulizer fails to nebulize a aqueous solution due to the disturbance by electrostatic forces in the pinch off process.

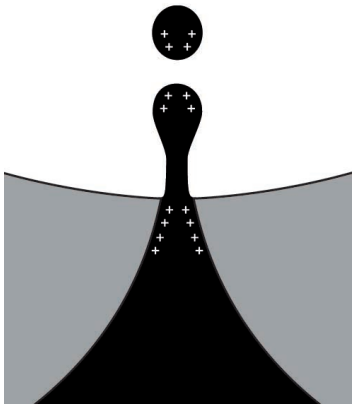

Figure 2.11: The hypothesis that the nebulizer fails to nebulize a aqueous solution due to the repulsion of the second droplet back into the nozzle by the electrostatic forces exerted on it by the first droplet.

Chapter 3

Method

3.1 Solution preparation

The experimental work during this research was majorly concerned with different types of solutions, such as electrolyte solutions. As was discussed in section 2.4, the motivation of this research even revolved around a solution: a sodium-chloride solution. It is therefore discussed here how the solutions used during the experiments were produced.

Three electrolyte solution where used, each with different molarities, varying from 0.01 mM up to 1 mM. All of the electrolyte solutions where produced the same way. A 1 mM solution was produced by dissolving a certain amount of salt (sodium-chloride, calcium-chloride of iron(III)-chloride in one litre of DI water. The precise amount of salt required follows from the molar mass of each salt and the required concentration, and is determined as follows:

$$m_{salt} = c \cdot V_{H_2O} M_{salt} \tag{3.1}$$

where c is the required concentration, V_{H_2O} is the required volume of the solution and M_{salt} is the molar mass of the salt used for the solution.

The 1 mM solution is diluted with DI to obtain the other electrolyte concentration, so for example to obtain the 0.7 mM solution, 35 mL of the 1 mM solution is dilute with 15 mL of DI water.

Besides the electrolyte solutions, three solutions of Pluronic F-127 are used when looking into the surface tension dependency. Pluronic F-127 is a nonionic surfactant, which can lower the surface tension of a liquid. The critical micelle concentration (cmc), the concentration which provides the lowest possible surface tension of the liquid, is 950 to 1000 ppm. The cmc causes the surface tension of DI water to go down to approximately 37 $\mathrm{mN{\cdot}m^{-1}}$ (Perez-Toralla et al., 2013). For the experiments, three solutions where used, a solution with 10 percent of the cmc, a solution with 50 percent of the cmc and a solution with two hunderd percent of the cmc. For each of these solutions, 100 mL was required, so the amount of Pluronic F-127 required follows from dividing the cmc value by 10^4.

Most experiments were conducted with the solutions at room temperature. However, where required, the temperature was increased by placing a closed container with the solution in a water bath with the required temperature. After waiting the appropriate time, the solution then obtained the same temperature as the water bath.

3.2 Mass flow rate measurements

To investigate the influence of electrostatic and -kinetic effects on the formation of droplets, a first set of experiments was designed. The experiment measures the mass of the nebulizer over a certain time period, while it is turned on. The decline in weight over time gives the mass flow rate of the nebulizer.

From the theory it follows that the Debye length of an electrolyte solution is dependant on both the concentration of electrolytes and the valence of the electrolytes. A plot of the Debye lengths for different concentrations of different electrolyte solutions can be found in Figure 2.7. To test the hypothesis that there is a relation between the Debye length of a solution and the mass flow rate when nebulizing this solution, different concentrations of the different electrolytes from Figure 2.7 solutions where nebulized.

Beck-Broichsitter et al. (2014) already showed that for different concentrations of sodium-chloride, the mass flow rate, or output rate as they called it, of the nebulizer varies strongly. To confirm this result, the experiment from Beck-Broichsitter et al. (2014) was repeated by a team of Bachelor students under the supervision of the author. These Bachelor students also expanded this experiment by varying the concentration of a calcium-chloride solution. On their experiment was expanded, by the author, to include the mass flow rate of different concentrations of ion(III)-chloride.

In these three experiments, the mass flow rate was determined for all the solutions found in Table 3.1.

Table 3.1: All the solutions for which the mass flow rate when nebulizing each solution was determined. 'x' indicates that a certain solution is used.

	NaCl	**CaCl2**	**FeCl3**
0.01 mM	x	x	x
0.02 mM	x	x	x
0.05 mM	x	x	x
0.07 mM	x	x	x
0.1 mM	x	x	x
0.2 mM	x	x	x
0.5 mM	x	x	x
0.7 mM	x	x	x
1 mM	x	x	x

The mass flow rate of the nebulizer when using different electrolyte solutions is determined by weighing the nebulizer over time while it is in working. The decrease in weight over time gives the mass flow, or output rate as Beck-Broichsitter et al. (2014) called it, of the nebulizer. A picture of the side view of the set-up can be found in Figure 3.1, and its schematic can be found in Figure 3.2.

The exact procedure was as follows: to ensure the nebulizer was clear of any residuals from the previous experiment, the reservoir of the nebulizer was rinsed 3 times with DI water, the nebulizer was turned on with DI water, and then rinsed again 3 times with DI water. After the cleaning procedure, the experiment could be performed. The nebulizer was placed in the holder, and the holder was placed on the scale, as can be seen in Figure 3.1. The cable of the nebulizer was attached to the nebulizer, the solution was added to the reservoir, and a few seconds where waited to ensure the scale was stabilised. When the scale was stable, the nebulizer was turned on. After the nebulizer was turned on, the scale was set to transfer the weight to the computer every second for two minutes. After these two minutes, the nebulizer was turned off and the process could be repeated for the next solution. The solutions where tested in ascending order of the amount of sodium-chloride in the solution, so starting with the 0.01 mM solution and ending with the 1 mM solution. This was done to limit the effect of possible residue in the reservoir of the previous solution. This series was repeated 3 times to minimize human and measurement errors, so for each solution 3 mass flow rates where determined.

Each measurement consisted of 120 data points, the weight of the total system at that point in time. These data points where plotted, and a clear linear relation could be seen in the data, as can be seen in Figure 4.1. Therefore a linear regression analysis was done on one measurement, where the slope of

the linear regression represented the mass flow rate of the nebulizer during that measurement. Doing this analysis for all three measurements at a given concentration, gave an average mass flow rate of concentration, together with a standard deviation. For each solution, so the different molarities but also the different electrolytes, this average mass flow together with the standard deviation was plotted in a single graph, as presented in Figure 4.2.

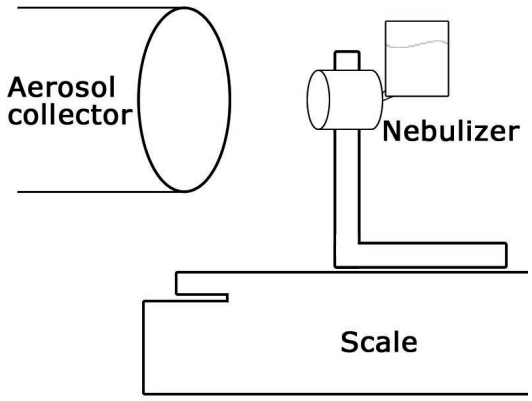

Figure 3.1: A schematic of the front view of the experimental set-up of the mass flow rate experiments.

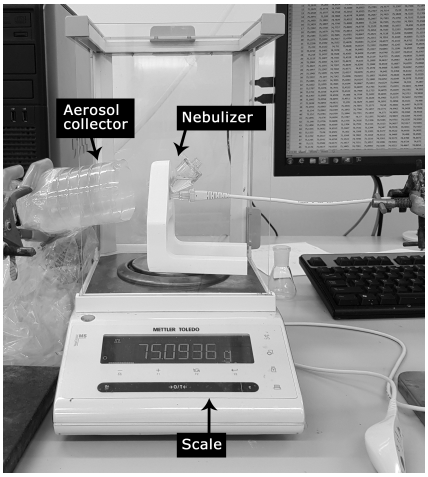

Figure 3.2: The experimental set-up of the mass flow rate experiments, looked at from the front. The nebulizer is placed in the holder, and the holder is placed on the scale. In the background the computer can be seen at which the data from the scale was collected.

3.3 Imaging

Looking at what happens at the end of the nozzle during the formation of a droplet can give more insight into the process. Therefore, images where obtained of the process at various speeds and magnifications.

A droplet is formed at the end of a tube with a diameter of 4.3 micrometer and leaves the tube at a speed with an order of magnitude of 1 $m \cdot s^{-1}$. To make images of this process, a high speed camera was required. Therefore a set-up was created, which is described in detail below. After this description it is explained how the set-up was used to obtain images, and what post-processing was done on these images.

3.3.1 Set-up

The camera set-up consisted of different parts, which are listed below with a description of their important features. A schematic overview of the set-up can be found in Figure 3.3, and an image of the actual set-up can be found in Figure 3.4.

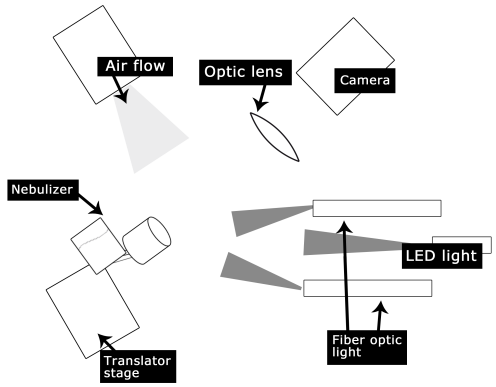

Figure 3.3: A schematic of the top view of the experimental set-up of the imaging experiments.

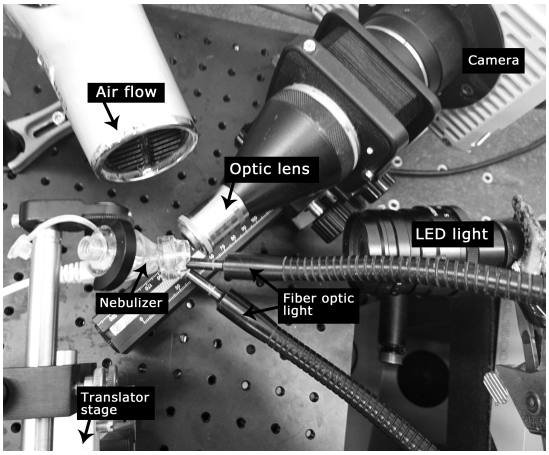

Figure 3.4: The experimental set-up of the imaging experiments, looked at from above.

Camera

The camera that was used is a Photron FASTCAM-APX RS, a high-speed camera that can go up to 3,000 frames per second at full resolution of 1024 x 1024 pixels, and up to 250,000 frames per second at a maximum resolution of 128 x 16 pixels (Pho, 2006).

The camera works with a 8 GB internal storage during imaging, resulting in a maximum of up to 30 seconds of imaging, depending on the frame rate and resolution. After imaging the acquired images can be reviewed in the internal camera storage using the Photron FASTCAM viewer software on a computer. The part of the imaging that is of interest can then be downloaded from the camera onto the computer.

The images can be downloaded in different forms, for example as an AVI movie or as seperate PNG images for each recorded frame. For ease of working with and editing of the images, they where downloaded as a PNG image for every recorded frame.

Optics

Three different lenses where used during the imaging, a 1x lens for the macroscopic images of the whole mesh, a 5x microscopic lens for the images of parts of the mesh and a 10x microscopic lens for the single nozzle images.

The 1x lens is a Sigma 105mm F2.8 lens (sig), which is used at the 1:1 zoom configuration. The 5x and 10x are both High Performance ZEISS Objectives for Microscopy (zei).

Lighting

Two light sources where used to meet the amount of light required at the maximum frame rate and minimal exposure time used during this research project.

The major part of the light came from a Schott KL 1500 Electronic Light Source, which is a fiber optic illuminator that transfers the light from a halogen, 150 watts lamp via two seperate fiber bundles to the object to be illuminated.

Since the material of the mesh is metal, and due to the geometry of the mesh, the light that is shone upon it reflects from the mesh as bright spots. To dissipate this effect an extra light source is added. This light source is Thorlab' MCWHL5 Mounted LED, a 800 mW LED light source. A simple lens system bundles the light emitted from this LED.

Air flow

To prevent the created droplets during nebulization to fog the lens, an airflow was created perpendicular to the lens. A 2000 W commercial hair-dryer was used for this purpose, since it is capable of creating a constant air stream of a relatively high air speed.

Translator stage

To obtain stable and sharp images, it was required to clamp the nebulizer, while also being able to translate it in 3 directions. For this, a translator stage was used. This translator stage was able to move in 3 directions, and on top of this translator a holder is placed for the nebulizer. In principle, while doing for example a series of measurements that require the same area of focus, the nebulizer can be removed and placed back without large adjustments of the translator stage.

3.3.2 Imaging procedure

To obtain images, the following procedure was performed: Firstly the nebulizer was rinsed in the same manner as described in section 3.2. The nebulizer was then placed in the holder on top of the translator stage and the lights where switched on. The camera was set at the desired frame rate with the software. The software allowed for a live feed from the camera, so this feed was used to bring the area of interest into focus by moving the nebulizer with the translator stage. When the image was in focus, the solution was added to the reservoir of the nebulizer and the airflow was turned on. The camera was switched on via the software, and lastly the nebulizer was turned.

When the images where made, they where first stored locally on the camera to be able to store the images at such a high frame rate. This gives to opportunity to have a first look into these images, via the software. When the desired images from the entire clip where selected, they where downloaded onto the computer.

3.3.3 Image editing

The images downloaded from the camera where PNG file, all containing a number representing their position in the sequence. These image numbers, together with the frame rate, lead to the time between images, which can be used to determine the time for certain processes to take place.

Some of the obtained images where usable right away, but most of them required cropping, rotating or adjustments in brightness or contrast. This was done using the ImageJ software (Ima). This software has the advantage of handling large amounts of images in sequence very well.

Chapter 4

Results

4.1 Mass flow rate measurements

As described in section 3.2, to test the hypothesis that there is a relationship between electrostatic and -kinetic effects and the performance of the nebulizer, solutions of different electrolytes where nebulized. The solutions varied both in concentration and in types of electrolytes, leading to different Debye lengths for each solution.

The result of a series of three measurements, each measurement using the same electrolyte solution, can be found in Figure 4.1. Each measurement represents the decline in weight of the nebulizer when it is switched on. As can be seen in the figure, the decline in weight appears to be linear. A linear regression analysis was done using Excel (Microsoft Corporation), which determines the slope of the decline in weight. This slope represent the mass flow rate of the nebulizer with this specific electrolyte solution. This experiment was repeated three times for each specific solution, and these three measurements can be seen in Figure 4.1. This resulted in three different mass flow rates for the same solution. From these three measurements the average mass flow was determined, together with the standard deviation of these three measurements.

The graph in Figure 4.1 was produced for each of the solutions as described in section 3.2. Each of these series of three measurements produced an average mass flow rate of a specific solution, together with the standard deviation of these three measurements. The result of all of the average mass flow rates and the standard deviations can be found in Figure 4.2. Not depicted in Figure 4.2 but still measured is the mass flow rate for nebulizing DI water. This mass flow rate is 0.011 g/min, with a standard deviation of plus and minus 0.0091 g/min. For comparison: the lowest mass flow rate measured for the different solutions was that of 0.01 mM sodium-chloride, and was 0.058 g/min, so still 5 times higher than the mass flow rate when nebulizing DI water.

The first thing that stands out in Figure 4.2 is the resemblance between the mass flow rates of sodium-chloride in this experiment and the mass flow rates found by Beck-Broichsitter et al. (2014). Roughly the same jumps in mass flow rate are found when increasing the concentration of sodium-chloride from 0.01 mM to 1 mM, indicating the results are obtained in a similar matter as the results found by Beck-Broichsitter et al. (2014), and can be subjected to the same conclusions. The mass flow rate found in the measurements with sodium-chloride are lower than the mass flow rates found by Beck-Broichsitter et al. (2014). This is likely due to the different model of vibrating-mesh nebulizer used in the different cases. The s-shape of the data points is roughly the same for both cases, which leads to the conclusion that the results from both cases are similar.

The second thing that stands out is the noticeable difference in mass flow rate between the sodium-chloride solution and the other two electrolyte solutions. This confirms the hypothesis that not only the concentration of the electrolyte solution has an influence on the Debye length and therefore the mass flow rate, but the valance of the species in the electrolyte solution has an influence as well. Both the calcium-

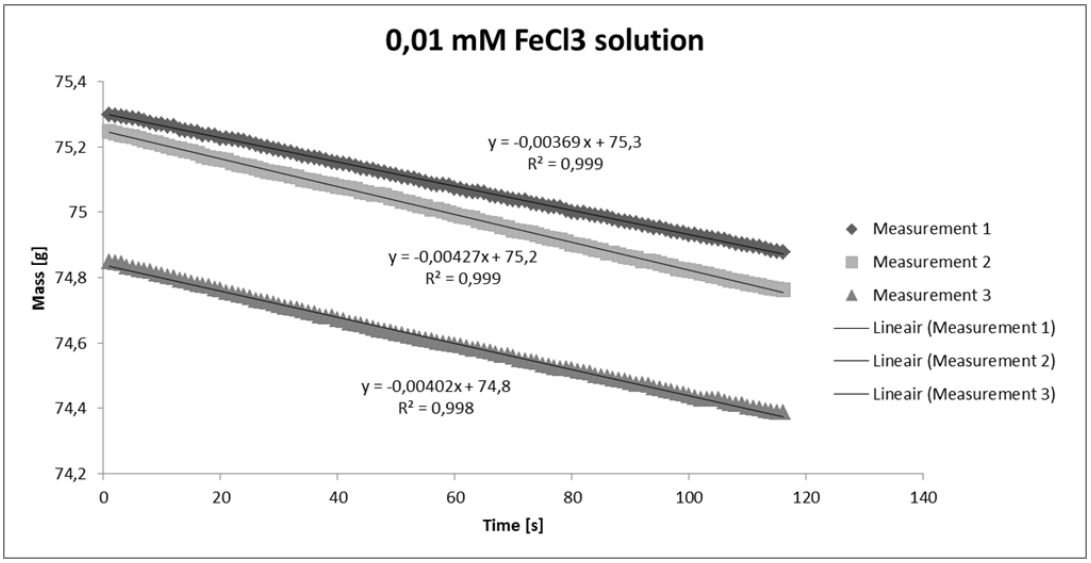

Figure 4.1: The results from three separate measurements of the decrease in mass over time for the nebulization of a 0.01 mM iron(III)-chloride solution.

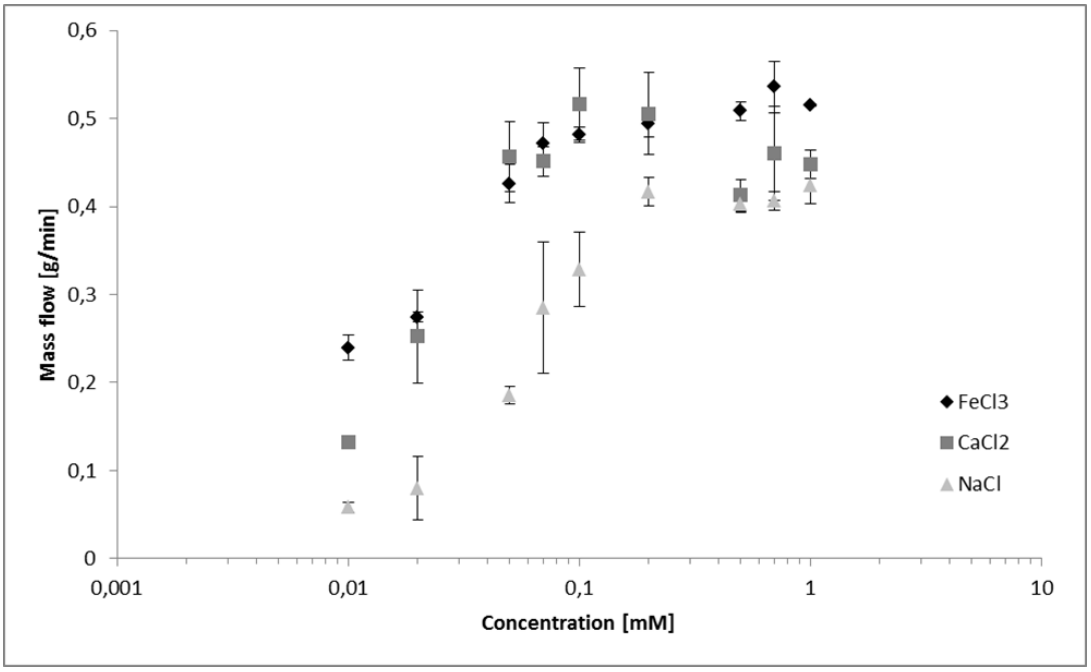

Figure 4.2: The average mass flow rate of three different types of electrolyte solutions, sodium-chloride, calcium-chloride and iron(III)-chloride. The mass flow rate of different concentrations of each of these electrolyte solution was measured three separate times, the average of these three repetitions is shown here, together with the standard deviation of the three repetitions.

chloride and the iron(III)-chloride show the same shape of data points with increasing concentration as the sodium-chloride data points, but at the same concentration have a higher mass flow rate than the sodium-chloride solution.

However, the third notable point which can be seen in Figure 4.2 is that there is no noticeable difference between the mass flow rates of the calcium-chloride and the iron(III)-chloride solutions, with the exception of both solutions at a concentration of 0.01 mM. This lack of difference in mass flow rate between the two electrolyte solutions can be explained by the simplifications that are made in the theory for the behaviour of the ions in the electrolyte solutions. The research by Ivan Guerrero-Garcia and Olvera de la Cruz (2014) found that models describing the electric double layer require modifications for multivalent ions. In the research done by Ivan Guerrero-Garcia and Olvera de la Cruz (2014), it showed that this is in particular true for trivalent ions. This might explain why there is little notable difference in mass flow rate between the calcium-chloride and the iron(III)-chloride solutions.

4.2 Imaging

The results in section 4.1 confirmed there is an influence of electrostatic and -kinetic effects on the formation of droplets, but it does not show in what way it influences the formation of droplets. To gain further insight into the way these effects influence the formation of droplets, images at different magnifications and frame rates where taken as described in section 3.3. Any differences in brightness and contrast between images taken at the same magnification are due to small variations in the positioning of the lighting between experiments. These differences are attempted to be minimized by adjusting brightness and contrast levels during the editing of the images.

4.2.1 Imaging the whole mesh

As a start, the whole mesh was imaged during the nebulizing process to get a proper look at the macroscopic events that take place during nebulizer operation. It was found that for the solutions that do not reach a maximum mass flow rate i.e. low salt concentrations as can be seen in Figure 4.2, a liquid film forms on the mesh in a periodic manner. Liquid builds up on the holder around the mesh, seems to reach a critical point, and covers the mesh in a matter of microseconds. When the liquid film covers a certain area of the mesh, the liquid then drains from the mesh into the nozzle of the nebulizer. When the mesh is free of the liquid film, the process starts again with accumulation of liquid at the holder around the mesh. The formation of this liquid film does not happen when the nebulizer has the maximum mass flow rate, so it can be assumed that the liquid film is related to the failure mode that occurs when nebulizing.

An example of a few consecutive periods of the formation of the liquid film can be seen in Figure 4.3 until Figure 4.8. Figure 4.3 and Figure 4.4 show the first period, Figure 4.5 and Figure 4.6 show the second period and Figure 4.7 and Figure 4.8 show the third period. The images show the periods of the formation of this liquid film and the draining that follows. All the images show the holder of the mesh, recognised by the serial number on its surface, and the mesh itself, recognised by the pattern of small holes covering the surface. The direction of gravity is indicated with a white arrow in the bottom left corner, and the white scale bar in the bottom right corner indicates the scale of the image.

The liquid buildups on the mesh have a different shape for each different period in this series. As can be seen in Figure 4.4, only a small area on the bottom of the mesh is covered. The second time the liquid buildup takes place, the bottom half of the mesh is covered, as can be seen in Figure 4.6. The final liquid film that is formed in this series covers the entire mesh, as can be seen in Figure 4.8. This series might suggest that the amount of area that is covered by the liquid film increases with every period, but this is not always the case. In Appendix B, series of periods of the 0.01 mM and 0.05 mM sodium-chloride solution nebulizations can be found, where it can be seen that the amount of area that is covered by the liquid films appears not to be periodic.

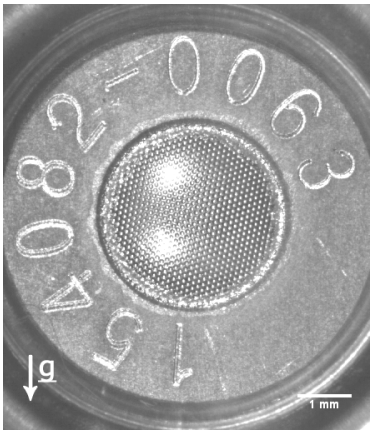

Figure 4.3: Nebulization of DI water, a macroscopic view at t=0 s

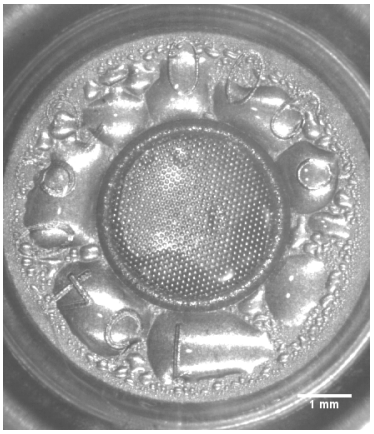

Figure 4.4: Nebulization of DI water, a macroscopic view at t=2.58 s

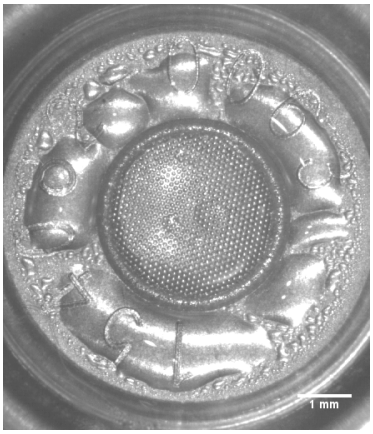

Figure 4.5: Nebulization of DI water, a macroscopic view at t=3.33 s

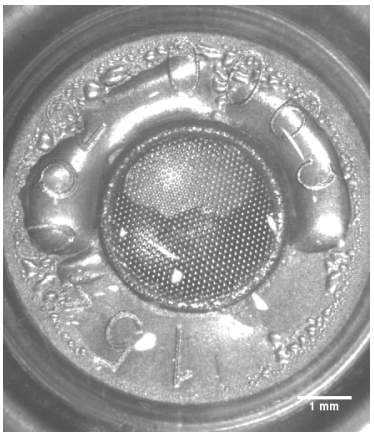

Figure 4.6: Nebulization of DI water, a macroscopic view at t=4.19 s

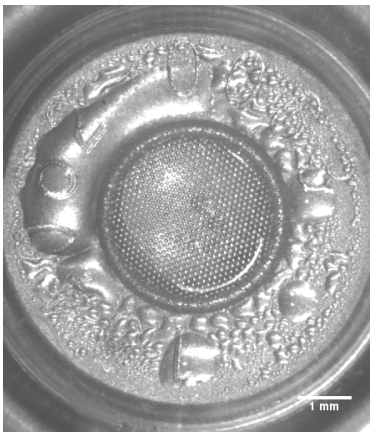

Figure 4.7: Nebulization of DI water, a macroscopic view at t=5.23 s

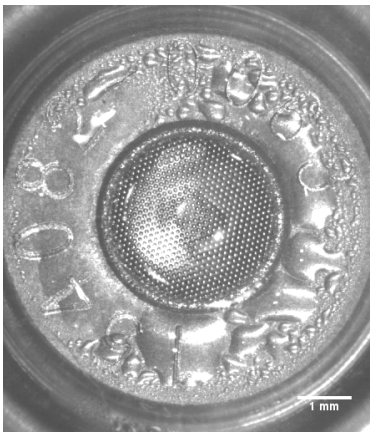

Figure 4.8: Nebulization of DI water, a macroscopic view at t=6.20 s

This periodic process repeats itself every couple of seconds for all these solutions. What differs greatly between the solutions is the time it takes for the liquid film to form on the mesh, which increases with increasing molarity of sodium-chloride in the solution. This is especially noticeable for the first period, the period shown in Figure 4.3 and Figure 4.4, so the formation of the first liquid film after the nebulizer is turned on. To quantify this, the time to form the first liquid film is determined for DI water and the sodium-chloride solutions. The result can be seen in Figure 4.9. It shows the average time to form the first liquid film from three repetitions of experiment with the same solution, together with the standard deviation of these three experiments.

What is noticeable is the buildup of liquid on holder of the mesh. As time goes on, liquid pools form on this surface, increasing in size over time. The only way for liquid to go from the reservoir of the nebulizer to the side of the mesh that is in the images is through the mesh, so the liquid that accumulates on the holder of the mesh is liquid that comes from the reservoir, via the mesh.

It appears that these liquid pools reach a certain critical size, before collapsing (partly) onto the mesh. An example of such a collapse can be seen in Figure 4.10 to Figure 4.15, and shows the collapse when DI water is nebulized.

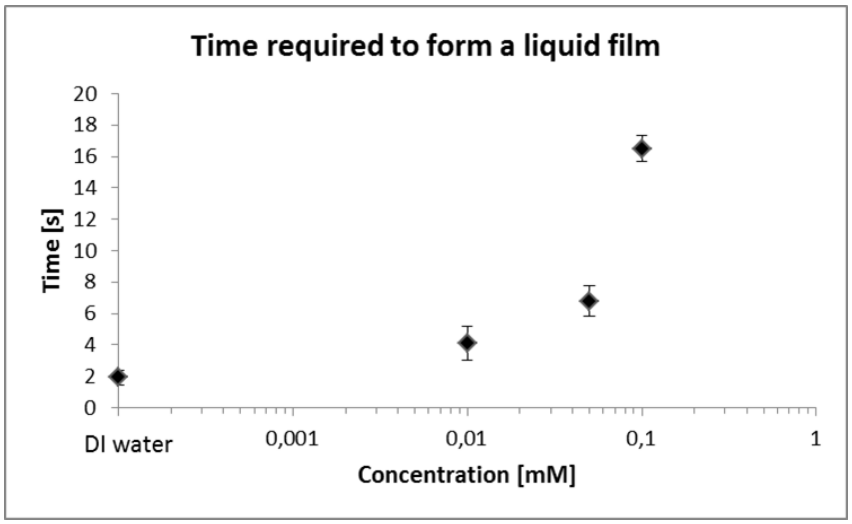

Figure 4.9: The time required for the first liquid film to collapse onto the mesh. An increase of this time can be seen for an increase in sodium-chloride concentration.

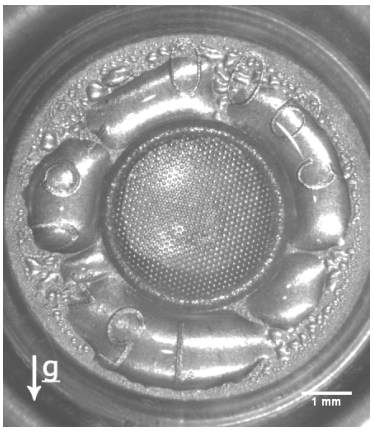

Figure 4.10: Nebulization of DI water, a macroscopic view at t=0 s

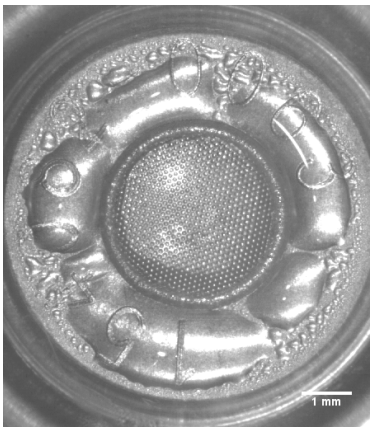

Figure 4.11: Nebulization of DI water, a macroscopic view at t=0.004 s

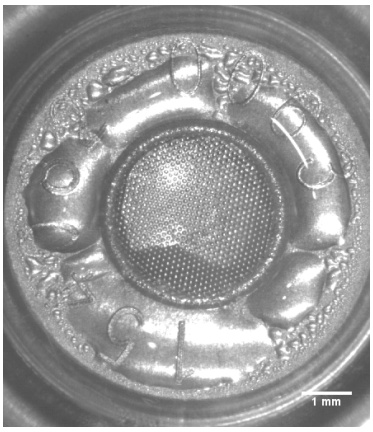

Figure 4.12: Nebulization of DI water, a macroscopic view at t=0.008 s

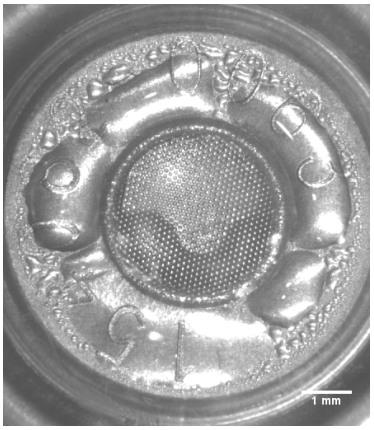

Figure 4.13: Nebulization of DI water, a macroscopic view at t=0.012 s

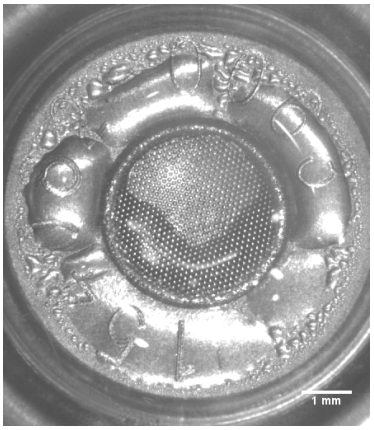

Figure 4.14: Nebulization of DI water, a macroscopic view at t=0.016 s

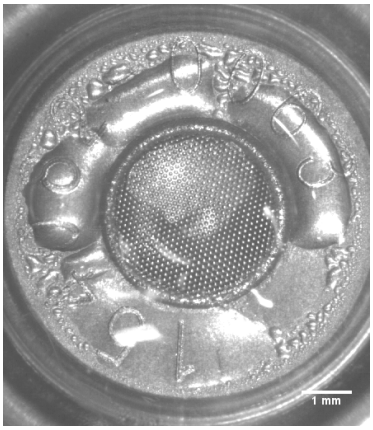

Figure 4.15: Nebulization of DI water, a macroscopic view at t=0.02 s

4.2.2 Imaging a single nozzle

The images investigating the liquid film that forms on the mesh gave an insight into the macroscopic movement of this film, but could not show how this film forms from the liquid that comes from the nozzles in the mesh. Therefore, a closer look at a single nozzle in the middle of the mesh, at an higher frame rate is taken. In subsection 2.1.3 it was estimated, when the nebulizer is at is maximum mass flow rate, that for every oscillation of the mesh, every nozzle in the mesh produces a single droplet. This indicates that droplets form with a frequency of oscillation of 128 kHz. Translating this to a time scale, one droplet forms every 1/128000 seconds, which is one droplet roughly every 7.8 μs.

The images from Figure 4.16 show the formation of the first droplets after the nebulizer is turned on to nebulize DI water, the top left is the first image of the process, the bottom right is the last image of the process. The images were taken at a frame rate of 250,000 frames per second, so the time between each image is a little less than half the oscillation of the mesh. What can be seen in the images is a single nozzle in the mesh, magnified 10 times. The black dot in the middle of the images, most clearly seen in the first image from Figure 4.16, is the nozzle in the mesh. The direction of gravity is indicated with a white arrow, and the white scale bar indicates the scale of the images.

Looking at the images for DI water, the formation of droplets can clearly be seen. In the second image the first signs of a droplet forming at the nozzle can be seen. The black arrow in the images show the movement of a single droplet through the frame, until it is out of frame in the bottom right image. Assumed is that the same droplet can be seen in the frames. This shows that for DI water, the droplet moves slower than expected, if the expectation was one droplet per oscillation, so one droplet with every two frames.

Figure 4.16: Eight consecutive frames at 250,000 frames per second of a single nozzle, while nebulizing DI water

Looking at the images from the nebulization of the 0.01 sodium-chloride solution in Figure 4.17, these images also show a droplet forming and moving outside the frame. Again the black arrows follow a single droplet as it moves through the frame.

Figure 4.17: Eight consecutive frames at 250,000 frames per second of a single nozzle, while nebulizing a 0.01 mM sodium-chloride solution

Figure 4.18 shows the same process again, but here it appears that a droplet forms, indicated by the black arrows on the top row of images. In the bottom row, the black arrows indicate the formation of a new droplet. This means two droplets form in the time span that these images where taken, instead of one, as was the case for the DI water and the 0.01 mM sodium-chloride solution.

Figure 4.18: Eight consecutive frames at 250,000 frames per second of a single nozzle, while nebulizing a 0.05 mM sodium-chloride solution

Figure 4.19 shows the formation of droplets for the 0.1 mM solution. The black arrows point to droplets moving through the frame. The frames between the frames with the black arrow appear to be empty. This means that in the span of 8 frames, 4 droplets have formed. This is in line with the expectation that one droplet forms with every oscillation, so with every two frames.

Figure 4.19: Eight consecutive frames at 250,000 frames per second of a single nozzle, while nebulizing a 0.1 mM sodium-chloride solution

In the images for the 1 mM solution in Figure 4.20, only the shape of two droplets can be seen, indicated by the black arrows. This could mean that only two droplets form in these 8 frames, but based on the maximum performance of the nebulizer for this solution, this is unlikely. Another explanation is that the droplets move out of the frame to fast to be visible at this frame rate.

Figure 4.20: Eight consecutive frames at 250,000 frames per second of a single nozzle, while nebulizing a 1 mM sodium-chloride solution

Comparing the formation of droplets for the different concentrations of salt in the solutions, it appears that, with increasing salt concentration, it is increasingly hard to see the droplets as they form and leave the nozzle. It is possible this is because the velocity of the droplet increases for increasing molarity, which makes it harder to get the image of the droplet sharp.

If the droplet formation process repeated itself identically in each period, images taken at a slightly higher or lower speed than the period could lead to images that show each step in the droplet formation, where the step size would be determined by the difference between the imaging speed and the speed at which the droplets form. To look into this possibility, images at various speeds where taken. Unfortunately, these results did not show clear signs of a periodic process.

Single nozzle after first droplets

While it is relatively easy to spot the first droplets that come out of a nozzle after the nebulizer is turned on, for all solutions there appears to be liquid accumulating on the surface of the mesh. This makes it impossible to distinguish the droplet formation after some time. Figure 4.21 to Figure 4.25 show a single nozzle after 0.012 seconds. What can be seen is that in this time, all of the solutions develop a large droplet of liquid on top of the nozzle. Since this happens for all solutions, which all have varying mass flow rates, this large droplet does not seem to prevent droplet formation.

Figure 4.21: A single nozzle after 0.012 seconds of nebulizing DI water

Figure 4.22: A single nozzle after 0.012 seconds of nebulizing a 0.01 mM sodium-chloride solution

Figure 4.23: A single nozzle after 0.012 seconds of nebulizing a 0.05 mM sodium-chloride solution

Figure 4.24: A single nozzle after 0.012 seconds of nebulizing a 0.1 mM sodium-chloride solution

Figure 4.25: A single nozzle after 0.012 seconds of nebulizing a 1 mM sodium-chloride solution

From the large droplet that accumulated on the exit of the nozzle, small droplets seem to be ejected, as can be seen in Figure 4.26. These images where taken at 14,000 frames per second. The black arrow points at a droplet that is ejected from the accumulated droplet at the nozzle exit.

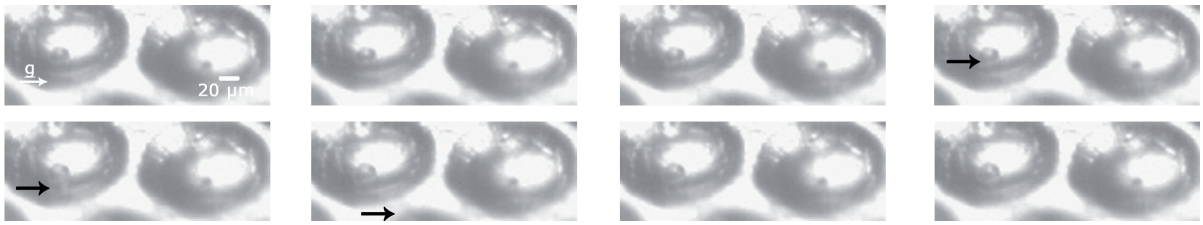

Figure 4.26: Eight consecutive frames at 14,000 frames per second of a single nozzle, while nebulizing a 1 mM sodium-chloride solution

4.2.3 Varying temperature and surface tension DI water

In section 2.4, the pressure to form droplets was determined, and the theory to determine this pressure showed a strong dependence on both the viscosity and the surface tension of the liquid. Therefore, it was of interest to have closer look at the influence of these parameters of the performance of the nebulizer. Using imaging to see what happens at the macro scale, some insight was gathered into this influence.

The viscosity of water is dependent on the temperature in the following way (Kundu et al., 2016):

$$\mu = 2.414 \cdot 10^{-5} \cdot 10^{247.8/(T-140)} \tag{4.1}$$

Where T is the temperature of water in degrees Kelvin. The viscosity of water at room temperature is 0.001 Pa·s^{-1} and the viscosity of water at 80 °C is 0.00035 Pa·s^{-1}. The viscosity can thus be lowered by a factor 3 by increasing the temperature of water by 60 °C.

DI water was heated in a warm water bath until it reached 80 °C. This warm DI water was added to the reservoir of the nebulizer and the nebulizer was turned on. While the DI water was added at a temperature of 80 °C, heat loss to the environment caused the actual temperature of the DI water while nebulizing to be around 60 °C.

To compare the operation using warm DI water to using DI water at room temperature, the occurrence of the first film was used as an indicator. Figure 4.29 shows the occurrence of the first film for DI water at room temperature at t=2.85 s. Figure 4.30 shows the nebulizer at the same time t=2.85 s, but now for warm DI water. What can be seen in Figure 4.30 is the start of the formation of the first film, however, this formation does not happen for another 2 seconds. Plotted in Figure 4.27 is the occurrence of the first film for both the DI water at room temperature and DI water at 60 degrees Celsius. To see if this occurrence happens at the same time, every time, the experiment was repeated 3 times. The average time of occurrence of the first film is plotted together with the standard deviation of the three experiments. In the plot it can be seen that there is a significant increase in the time to form the first liquid film. As was discussed in subsection 4.2.1, this time is an indicator for the performance of the nebulizer. From Figure 4.27 it can therefore be deducted that there is an increase in performance by the increase of temperature. Further interpretation of this result with regards to the influence of temperature of other properties of DI water will be discussed in chapter 5.

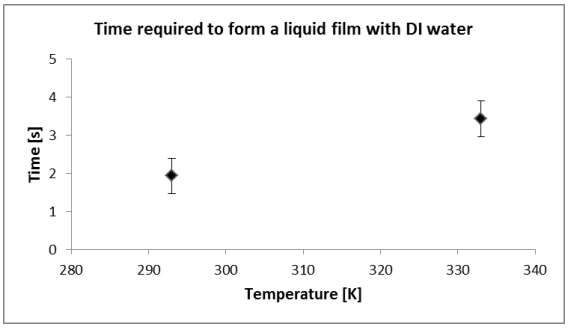

Figure 4.27: The time required for the first liquid film to collapse onto the mesh. An increase of this time can be seen for an increase temperature.

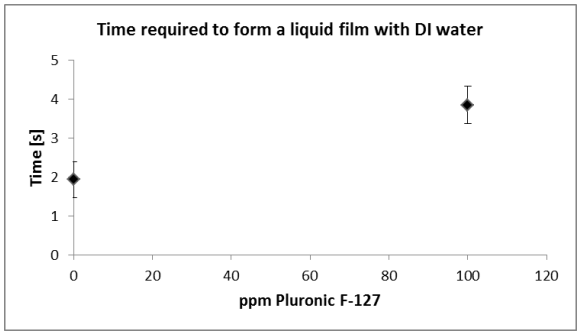

Figure 4.28: The time required for the first liquid film to collapse onto the mesh. An increase of this time can be seen for an increase in surfactant concentration.

To vary the surface tension of DI water, a nonionic surfactant called Pluronic F-127 was added to the DI water. As discussed in section 3.1, different amounts of surfactant where added to the DI water to influence the surface tension. The results can be seen in Figure 4.31 to Figure 4.34. Figure 4.31 shows the occurrence of the first film for DI water without surfactant (so at a surface tension of 72 $mN \cdot m^{-1}$) at t=2.85 s. Figure 4.32 shows the nebulizer at the same time, but now with 100 ppm or 0.1 times the cmc value of added Pluronic F-127, so with a surface tension of approximately 45 $mN \cdot m^{-1}$ (Perez-Toralla et al., 2013). Figure 4.33 and Figure 4.34 show the nebulizer at the same time, but now with 0.5 and 2 times the cmc value, resulting both in a surface tension of 37 $mN \cdot m^{-1}$.

The addition of surfactant to DI water had a significant influence on the time to form the first liquid film. At a surface tension of 45 $mN \cdot m^{-1}$, so adding 0.1 times the cmc value of surfactant, the time to develop the first film increases by roughly two seconds, as can be seen in Figure 4.28. Again the experiment was repeated three times, and plotted in Figure 4.28 is the average time to form the first film and the standard deviation of these three measurements. At a surface tension of 37 $mN \cdot m^{-1}$, so for both the 0.5 times and 2 times the cmc value added to DI water, there is no formation of a liquid film at all. These results indicate an increase in performance for a decrease of surface tension. Further interpretation of this result with regards to the influence of the surfactant of other properties of DI water will be discussed in chapter 5.

Temperature

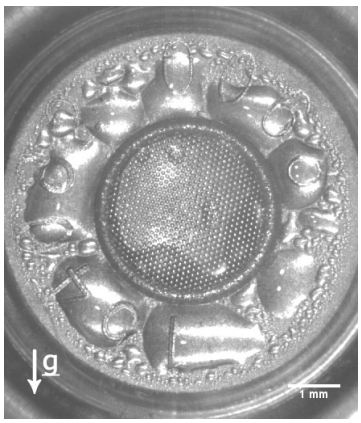

Figure 4.29: Nebulization of DI water, a macroscopic view at t=2.85 s with a temperature of 293 K

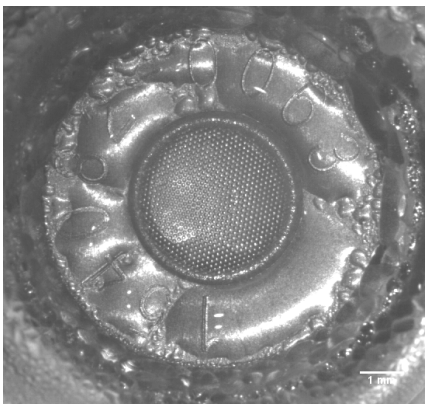

Figure 4.30: Nebulization of DI water, a macroscopic view at t=2.85 s with a temperature of 353 K

Surface Tension

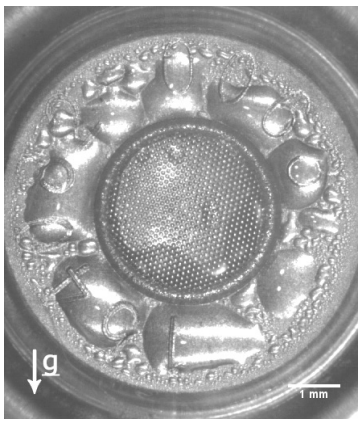

Figure 4.31: Nebulization of DI water, a macroscopic view at t=2.85 s

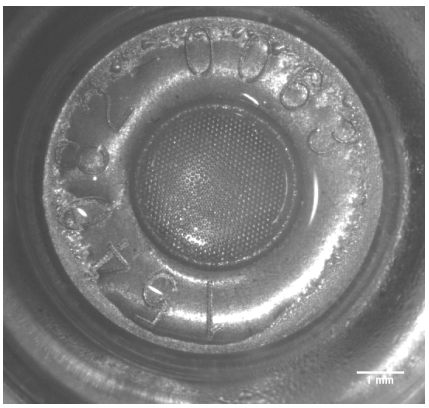

Figure 4.32: Nebulization of DI water, a macroscopic view at t=2.85 s with 0.1 times the cmc value of the surfactant added

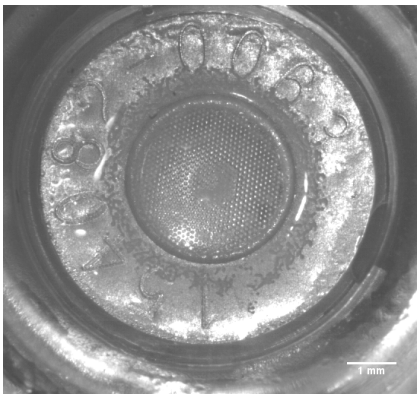

Figure 4.33: Nebulization of DI water, a macroscopic view at t=2.85 s with 0.5 times the cmc value of the surfactant added

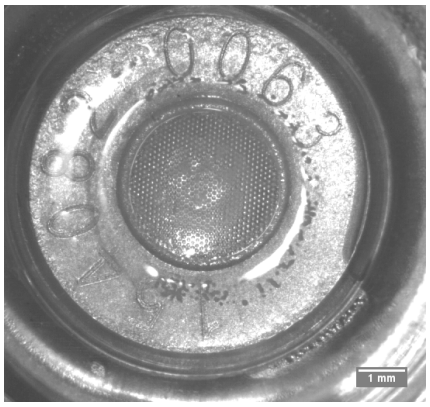

Figure 4.34: Nebulization of DI water, a macroscopic view at t=2.85 s with 2 times the cmc value of the surfactant added

Chapter 5

Discussion

The theory combined with the results of the experiments leave a lot to be interpreted, and are also not without it its limitations. Both of these topics are discussed here, starting with the interpretation of the results and the connection to theory, followed by the limitations of this research.

5.1 Interpretation of the results

The results in chapter 4 provide a lot of different findings to be interpreted. Starting at the mass flow rate, this experiment showed both expected and unexpected results. As expected, the sodium-chloride curve showed strong resemblance to the results by Beck-Broichsitter et al. (2014). Based on the hypothesis that the electrostatic and -kinetic effects influence the mass flow rate, the Debye length serves as a measure for these effects and the theory to determine the Debye length, the fact that calcium-chloride and iron(III)-chloride curves where higher in mass flow rate than the sodium-chloride curve was an expected result. Unexpected was the lack of significant difference between the calcium-chloride and the iron(III)-chloride curves. When having a closer look at the theory regarding multivalent electrolyte solutions as discussed in section 4.1 however, this result could be explained. The results from the mass flow rate where a confirmation that indeed electrostatic and -kinetic effects have an influence on the process of droplet formation.

The imaging results lead to a number of interpretations. Starting with the macroscopic imaging results, the formation and collapse of the liquid film onto the mesh is an interesting process. The liquid that accumulates on the holder can not come from anywhere else than the reservoir of the nebulizer, via the mesh. Before imaging, it was not exactly clear what happened to the liquid that was not nebulized, when nebulizing solutions with low salt concentrations. The accumulation of liquid on the holder indicates that at least part of the liquid that is not nebulized properly passes through the nozzles of the mesh. How this liquid moves from the nozzles to the holder is not visible in the macroscopic images, but a quick computation can give an indication how much liquid accumulates on the holder.

Taking as an example the formation of the first liquid of the 0.01 mM sodium-chloride solution. The mass flow rate of this solution is 0.06 grams per minute, while the maximum mass flow rate with the 1 mM solution is 0.42 grams per minute. This means there is 0.36 grams per minute unaccounted for. Also determined is that the first liquid film that forms collapses after 4.11 seconds. The maximum area that can be covered is the area of the holder of the mesh, which has an area of 15.9 mm^2. The maximum height of the film can be determined using an approximation of the liquid pool on the holder as a sessile drop, where the maximum height is determined by the force balance of the surface tension forces and the pressure forces. The maximum height can be determined by:

$$H_{\max} = 2l_{cap} \sin\left(\frac{\theta}{2}\right) \tag{5.1}$$

where θ is the contact angle between the liquid, the solid and the gas phase, and l_{cap} is the capillary length determined by:

$$l_{cap} = \sqrt{\frac{\gamma}{\rho g}} \tag{5.2}$$

Using the contact angle of water with aluminum, the maximum height of the film is 2.87 mm. Together with the maximum area the liquid can cover, this leads to a maximum of 45 mm^3 of liquid on the holder. Taking the time of collapse as a timescale for this liquid to build up, this would lead to a mass flow into the liquid film of 0.0016 grams per minute. Compared to the 0.36 grams per minute that the nebulizer does not nebulize, this is only 0.44 % of that. This suggest that only a very small part of the solution that was not properly nebulized ends in the liquid build up on the holder.

When the liquid film covers the mesh, the temporarily blocks (parts of) the mesh, and therefore lowers the mass flow rate of the nebulizer. However, the time the liquid film covers the mesh is much shorter than the time the mesh is free of any liquid. From this it can be suggested that the individual nozzles produce less mass flow when the overall mass flow rate is not at the maximum. Another interpretation can be that the total number of nozzles that function has decreased. This interpretation makes sense if when considering the shape of the mesh, a sketch of the cross-section during one oscillation can be seen in Figure 5.1.

Figure 5.1: The positive and negative excitement of the mesh during on oscillation

The excitement of the mesh is 1 μm (Aer), but since the mesh is clamped at the outer diameter, this excitement grows smaller towards the outer diameter. Since the pressure to produce droplets is induced by this excitement (together with the velocity of the mesh), the decreasing excitement towards the outer diameter of the mesh leads to a decreasing pressure towards the outer diameter of the mesh. When this decrease in pressure drops below the minimum required pressure to form droplets as computed in section 2.4, it causes the nozzles towards the outer diameter to be inactive. A sketch of the mesh during the formation and collapse of the liquid film can be found in Figure 5.2. In the first figure of Figure 5.2, a single nozzle on the outer diameter of the mesh is indicated. Figure 5.3 shows a schematic of this single nozzle during the nebulization of a solution with a low salt solution.

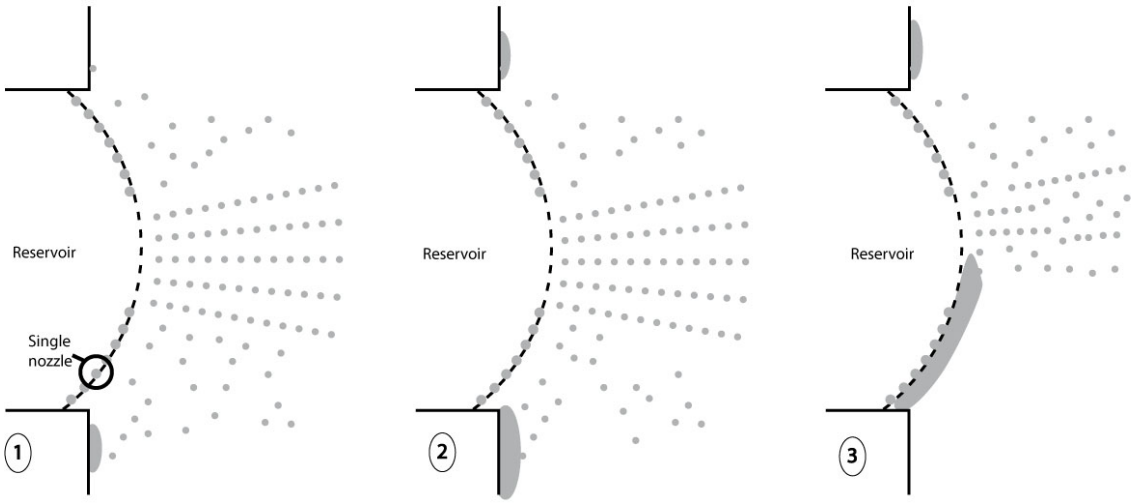

Figure 5.2: A schematic representation of the buildup of liquid on the holder and the collapse of the liquid onto the mesh.

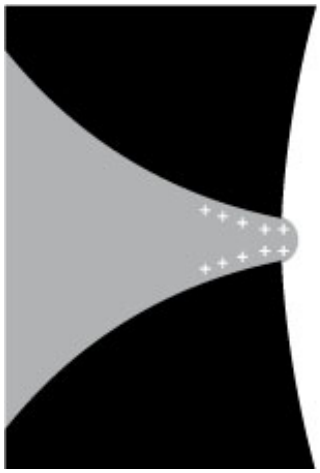

Figure 5.3: A schematic representation of what happens in the nozzle indicated in the first figure of Figure 5.2. The increased viscosity or the decreased effective diameter increase the pressure required to form a droplet at the exit of the nozzle, and therefore prevent a droplet from forming

The suggestion that individual nozzle perform less then optimal is supported by the images of the single nozzle as was seen in subsection 4.2.2. While it is hard to quantify, from these images it can be derived that the droplets form faster at higher mass flow rates. This is where the electrostatic and -kinetic effects must come into play. The electric double layer influences the flow through the nozzle in such a way that it decreases the mass flow through the nozzle. This effect is revered to as electroviscosity, and for channels where the diameter is of the same order of magnitude as the Debye length, can reduce the flow rate by as much as a factor of 1.3 according to Chun and Kwak (2003) or two according to Kirby (2013). No actual physical changes in the viscosity take place, rather the fluid through a microchannel such as the nozzle appears to be more viscous or the channel appears to have a smaller diameter.

If the flow through the nozzle experiences the equivalent of an increased viscosity of the fluid due to the electric double layer, the pressure required to form a droplet at the exit of the nozzle as computed in section 2.4 increases. Decreasing the viscosity of the liquid would be able to decrease this required pressure, thereby acting as a counterbalance to the effect of the electroviscosity. The experiment where

the temperature was increased supports this hypothesis. The increase in temperature, and therefore a decrease in viscosity, increased the performance of the nebulizer.

The experiment where the surface tension of the liquid was lowered, also indirectly supports this hypothesis. Decreasing the surface tension leads to a decrease in the pressure required to form droplets at the end of the nozzle. So while the pressure required to overcome the viscous effects in the nozzle increases, the pressure required to overcome surface tension forces decreases, mitigating this effect. This showed in the results in Figure 4.28, where the time to form the first liquid film increases, and for the lowest surface tension solutions tested, no liquid film formed at all.

When the flow rate through a single nozzle decreases, it is important to re-evaluate the process of droplet formation by looking again at the dimensionless numbers describing the process. The mass flow, or to be specific the velocity of the flow, was of influence of two of these dimensionless numbers: the Weber number and the Froude number. The Weber number becomes smaller when the velocity decreases, suggesting that the surface tension forces play an even larger role in the droplet formation process. The Froude number also decreases with a decrease in velocity, indicating that gravitational forces play a larger role in the movement of the droplet when it leaves the nozzle. This increase of influence of the gravitational forces might give an explanation why the liquid seems to build up faster on the bottom half of the holder than on the top half.

5.2 Limitations of the research

To have a sense of the scope of the results and its interpretation, it is important to indicate the limitations of this research. These limitations are discussed here.

Starting with the experiments itself, a couple of limitations can be noted. Firstly, while the effects of errors on the results was attempted to be kept at a minimum, some experiments could require more repetitions to filter out human and measurement errors. During this research, this was a trade-off between accuracy and time constraints. The ease of repeating the same experiment in the exact same manner differed from experiment to experiment. While the mass flow rate experiments where rather straightforward to repeat by following the procedure, the imaging experiments where more difficult. The nebulizer was removed from the set-up between experiments to be rinsed, and placed back into the set-up after this was done. However, removing and placing the nebulizer back into the set-up made alternation to the set-up on a millimeter scale. Since the images, especially those of the single nozzle, where concerned with distances of the micrometer scale, this made it hard to have the exact same nozzle in view for every experiment.

A limitation which arises with most experimental research, is the limitations posed by the equipment used. For example, a camera that can make images at a higher frame rate could give more insight into the droplet formation process, especially in the single nozzle imaging experiment.

The results of the imaging experiments had the limitation of being difficult to quantify. When comparing the performance of the nebulizer when nebulizing different electrolyte solutions looking at images can certainly improve the understanding of certain processes. During this research, there was attempted to quantify as much of the results as possible. For example the time to form the first liquid film was an important parameter when comparing different solutions. The limitation lies with the single nozzle imaging. Here it was attempted to compare each solution based on the velocity of the droplet that formed, but this was much less accurate than comparing the macroscopic images. This was due to the low resolution and limited sharpness of the images.

The experiments where properties of a fluid where altered also had its limitations, especially in the interpretation of its results. Taking for example the experiment to test the influence of viscosity on the performance of the nebulizer. Varying the temperature results in a change of viscosity, but also changes other properties of the fluid, hydrodynamic and electrostatic. It is therefore hard to distinguish which changing properties is the cause of the results of this experiment, or how their changes combine to result in a specific outcome of an experiment.

Some questions remained unanswered during this research, it was not possible to image and explain how the liquid from the mesh found its way onto the holder. While the hypothesis of electrowetting was proven to be false, since droplets do appear to form for DI water, the other two hypotheses where not proven to be true or false. A new hypothesis was formed based on the results of this research. Still, no definitive answer to the main question was found: why is a vibrating-mesh nebulizer not capable of nebulizing pure water?

Chapter 6

Conclusion

This research set out to find an answer to the question: why is a vibrating-mesh nebulizer not capable of nebulizing pure water? It was hypothesised that electrostatic and -kinetic effects influence the droplet formation process and therefore the mass flow rate of the nebulizer. Three different ways in which these effects influence the droplet formation were hypothesised, as described in section 2.4. The first hypothesis was that charged induced wetting causes the liquid from the nozzle to spread out over the surface at the end of the nozzle, instead of forming a droplet. The second hypothesis was that due to electrostatic forces in the neck of the droplet formation process, the neck is prevented to decrease in diameter, no pinch-off takes place and therefore no droplet is formed. The third hypothesis was that a droplet was formed, taking with it an electrostatic charge. The next droplet is then prevented from exiting the nozzle, by the electrostatic force the first droplet exerts on it. These hypotheses where based on engineering intuition, rather than experimental data.

Experiments with the mass flow rate of the nebulizer showed that decreasing the Debye length of an electrolyte solution increases the mass flow rate of the nebulizer. The results of these experiments were in accordance with the literature by Beck-Broichsitter et al. (2014) and Ghazanfari et al. (2007), and confirmed the hypothesis that electrostatic and -kinetic effects influence the mass flow rate of the nebulizer.

Macroscopic imaging of the whole mesh showed that liquid builds up on the holder around the mesh and collapses over the mesh in a periodic manner, with a time scale of the order of 2 up to 20 seconds. Computations of the time scale of this build up showed that this liquid does not account for the total difference in mass flow rate compared to a maximum mass flow rate. This indicates that the nozzles in the mesh do not have the same mass flow or not all nozzles are active, when concentrations of electrolytes decrease as when the concentration of electrolytes is sufficiently high. Images of a single nozzle in the middle of the mesh in subsection 4.2.2 did show that for every solution, there are droplets that form. subsubsection 4.2.2 showed that for every solution, after around a certain time of order of magnitude of 0.01 seconds, liquid accumulates on the mesh. The difference between the single nozzle images of the different solutions is the speed at which the droplets form and move out of the frame.

Based on the results of this research, the electrowetting hypothesis was proven to be false. Images looking at the droplet formation at a single nozzle showed that droplets always form, even for DI water. The other two hypotheses could not be proven false or true based on the results, but based on the imaging in section 4.2 and the interpretation of these images in section 5.1, a new hypothesis was formed. The new hypothesis states that due to the significantly large electric double layer in solutions with low salt concentrations, the flow in the nozzle experiences an increased viscosity or smaller diameter than the nozzle diameter. This decreases the flow rate through the nozzle, resulting in either droplets with a reduced velocity, of inactive nozzles. This decreases the mass flow rate of the nebulizer. This hypothesis was tested by increasing the temperature of the liquid, which results in a decrease of the viscosity. The results of this experiment as described in subsection 4.2.3 give the indication that the increased viscosity is a promising hypothesis.

Chapter 7

Recommendations

This research, not unlike most others, never appeared to be quite finished. This is why a number a recommendations can be made for further research. These recommendations are discussed below.

7.1 Improving the experiments

A major part of the difficulty to investigated the workings of the nebulizer came from its complexity. This is due, in large part, to the fact that it is an industrial applications, rather than a laboratory set-up. It was therefore much harder to make adjustments to the nebulizer where it was required. Making adjustments to the nebulizer or the experimental set-up to have more ease of excess and to improve certain results is consequently the first and foremost recommendation. To be more specific, a number of different improvement and changes are recommended, each with their own advantages.

7.1.1 Improving imaging set-up

Some of the equipment of the imaging set-up was used to their limit during this research. For example, the camera was used at the maximum frame rate of 250,000 frames per second. However, due to the small scale of 5 μm and the velocity of the droplets in the order of 1 $\mathrm{m{\cdot}s^{-1}}$, it remained hard to see exactly what was happening at the droplet formation process.

During this research, images of droplet formation where recorded at roughly two images per period of droplet formation. Camera's available from the same manufacturer as the camera used, have camera's that can go up to 2 million frames per second. This would lead to roughly 16 images per period of droplet formation. It is expected that this would give more insight in the process of droplet formation by a vibrating mesh. This however, is not possible without also scaling up the light available for imaging. As a rule of thumb, twice the frame rate requires twice the amount of light. So improving the camera equipment to allow for a higher frame rate is recommended together with the recommendation to increase the amount of light available.

7.1.2 Slowing down the system

The recommendation to increase the speed of the camera of course has a counterpart. It is also possible to get more images of a period of droplet formation by slowing down the process of which the droplet is formed. The mesh in the system vibrates at 128 kHz, and the mass flow and the amount of nozzles indicate that every oscillation a droplet is formed. If the frequency could be lowered, the same camera as used in this research, would be able to obtain more images per period than at the frequency of 128 kHz.

However, doing this is recommended with a side note. While there are different models of vibrating-mesh nebulizers that operate at different frequencies, it is unsure if this particular model still functions properly at a lowered frequency. The frequency of the oscillation of the mesh, together with the excitement of the mesh, create the pressure required to push the liquid out of the nozzle as droplets. By changing the frequency, the pressure obtained from the oscillation of the mesh might not be sufficient anymore to form droplets. Since purchasing a camera that can go to frame rates of 2 million frames per second, might be a lot more costly than purchasing a piezo controller to change the frequency of oscillation of the mesh. It is therefore recommended to pursue this adaption of the system.

7.1.3 Simplifying the nebulizer

Simplifying the nebulizer, for example isolating a single nozzle instead of looking at the whole system of the mesh with more than a thousand nozzles, could greatly improve the clarity of the nebulizer process. For example, recreating a single nozzle in a different environment, without other parts of the nebulizer blocking access in one way or more, would greatly increase the imaging possibilities. This can not be done of course, without proper reasoning and justification. It is therefore recommended that further research is done into possible simplification of the system.

Scaling an industrial application such as this, especially since it in concerned with multiphase flow, is not an easy task. Many different scaling factors would have to be considered, and there is no guarantee it will even be possible to scale this problem. It is therefore not a recommendation to increase the scale of the system to increase the ease of access to and visibility of the processes.

7.2 Solutions to the problem

Besides performing more research to find a more definitive answer to the question why the nebulizer fails to nebulize pure water, a few possible solutions to (partly) solve this problem can be recommended.

7.2.1 Increasing operating temperature

As was found as a first prove of concept for the newly proposed hypothesis, in chapter 5, increasing the temperature appears to be improving the mass flow rate of the nebulizer, when nebulizing DI water. It can therefore be recommended to use DI water of an higher temperature than room temperature, when nebulizing. This does require further research into the consequences of increasing the temperature.

As mentioned in subsection 4.2.3, by increasing the temperature of DI water, the viscosity decreases. It it hypothesised that this decrease in viscosity leads to an increase of the mass flow rate. However, increasing the temperature of DI water not only changes the viscosity, but changes many properties of the fluid, hydrodynamic and electrostatic and -kinetic. Therefore, a further investigation into the influence of temperature of the nebulizing process is recommended, before implementing the increased temperature into the precedure of nebulizing.

In the same section as the increases in temperature was investigated (subsection 4.2.3), the influence of adding a surfactant to DI water was investigated. However, this is not recommended as a solution to the problem, as it adds matter to the liquid and therefore is not a way to make it possible to nebulize pure water.

7.2.2 Coating the mesh

A significant portion of this research was concerned with alternating the properties of the liquid to influence the behaviour of the nebulizing system. Salt concentrations where increased or decreased, the temperature was changed and the surface tension was brought down. However, little time was spent on changing the properties of the solid material of the mesh. As was described in subsection 2.4.2, the

electrostatic and -kinetic effects do not only come from the liquid, but from the interaction of the liquid with the fluid. It is therefore recommended that alternation of the surface of the mesh, for example by applying a hydrophobic coating, is further investigated.

Coating the surface of in intricate surface such as the mesh poses its own challenges. To be able to apply the coating not only on the outer surface, but also on the insides of the nozzle, requires a particular coating and a particular method of applying the coating. Since the diameter of the nozzle is a parameter that can not be altered, the coating has to be a sufficiently thin layer on the surface as to not increase this diameter. The coating also has to be able to endure the ways the nebulizer is used in practise. All of these requirements lead to the recommendation that further research is done into the coating of the mesh.

Bibliography

Sigma 105mm f2.8 ex dg os hsm macro. `https://www.sigmaphoto.com/105mm-f2-8-ex-dg-os-hsm-macro`. Accessed: 07-09-2019.

Zeiss microscope objectives. `https://www.zeiss.com/microscopy/int/products/microscope-components/objectives.html`. Accessed: 07-09-2019.

Aerogen Solo System Intruction Manual. Aerogen.

A. Ari. Jet, ultrasonic, and mesh nebulizers: An evaluation of nebulizers for better clinical outcomes. *Eurasian Journal of Pulmonology*, 16:1–7, 2014.

P. W. Atkins. *Physical Chemistry*. W.H. Freeman Company, 1892.

M. Beck-Broichsitter, N. Oesterheld, M.-C. Knuedeler, W. Seeger, and T. Schmehl. On the correlation of output rate and aerodynamic characteristics in vibrating-mesh-based aqueous aerosol delivery. *International Journal of Pharmaceutics*, 461:34–37, 2014.

T. C. Carvalho and J. T. McConville. The function and performance of aqueous aerosol devices for inhalation therapy. *Journal of Pharmacy and Pharmacology*, 68:556–578, 2016.

E. Chemmalasseri. Numerical modelling of droplet formation in mesh nebulizers. Technical report, Delft University of Technology, 2012.

M.-S. Chun and H. W. Kwak. Electrokinetic flow and electroviscous effect in a charged slit-like microfluidic channel with nonlinear poisson-boltzmann field. *Korea-Australia Rheology Journal*, 15(2): 83–90, 2003.

R. Dalby and J. Suman. I nhalation therapy: technological milestones in asthma treatment. *Advanced Drug Delivery Reviews*, 55:779–791, 2003.

P. Drazin. *Introduction to Hydrodynamic Stability*. Cambridge University Press, 2002.

T. Ghazanfari, A. M. Elhissi, Z. Ding, and K. M. Taylor. The influence of fluid physicochemical properties on vibrating-mesh nebulization. *International Journal of Pharmaceutics*, 339:103–111, 2007.

R. J. Good. Contact angle, wetting, and adhesion: A critical review. *Journal of Adhesion Science and Technology*, 6(12):1269–1302, 1992.

Image Processing and Analysis in Java. ImageJ.

G. Ivan Guerrero-Garcia and M. Olvera de la Cruz. Polarization effects of dielectric nanoparticles in aqueous charge-asymmetric electrolytes. *The Journal of Chemical Physics*, 118(29):8854–62, 2014.

K. K. Jain. Drug delivery systems an overview. *Methods in Molecular Biology*, 437, 2009.

M. Jenny, J. Dusek, and G. Bouchet. Instabilities and transition of a sphere falling or ascending freely in a newtonian fluid. *Journal of Fluid Mechanics*, 508:201–239, 2013.

J. Jiang and S. I. Sandler. A new model for the viscosity of electrolyte solutions. *Industrial Engineering Chemistry Research*, 42(25):6267–6272, 2003.

B. J. Kirby. *Micro- and Nanoscale Fluid Mechanics: Transport in Microfluidic Devices*. Cambridge University Press, 2013.

C. Kleinstreuer and Z. Zhang. Airflow and particle transport in the human respiratory system. *Annual Review of Fluid Mechanics*, 42(1):301–334, 2010.

M. Kosmulski. The ph-dependent surface charging and points of zero charge. *Journal of Colloid and Interface Science*, 353:1–15, 2011.

P. K. Kundu, I. M. Cohen, and D. R. Dowling. *Fluid Mechanics*. Elsevier, 2016.

H. P. Le. *Progress and Trends in Ink-jet Printing Technology*. IS&T, 1999.

J. Le, M. Iannuzzi, A. Cuesta, and J. Cheng. Determining potentials of zero charge of metal electrodes versus the standard hydrogen electrode from density-functional-theory-based molecular dynamics. *Physical Review Letters*, 119(1), 2017.

C. Li and H. Lee. Density calculation of electrolyte solutions with the solution osmotic pressure. *Chemical Engineering Science*, 55(2000):655–665, 1998.

Microsoft Corporation. Microsoft excel 2010. URL `https://products.office.com/nl-nl/microsoft-excel-2010`.

R. L. Miller, W. L. Bardford, and N. E. Peters. Specific conductance: Theoretical considerations and application to analytical quality control. Technical report, Department of the Interior and U.S. Geological Survey, 1988.

F. P. Muchão and L. V. R. F. da Silva Filho. Advances in inhalation therapy in pediatrics. *Jornal de Pediatria*, 86(5):367–376, 2010.

H. Ohshima and H. Matsubara. Surface tension of electrolyte solutions. *Colloid and Polymer Science*, 282:1044–1048, 2004.

R. Oliemans. Lecture notes. In *Applied Multiphase Flows*. TU Delft Faculty of Applied Sciences, 2011.

R. S. Patil, V. R. Shaikh, P. D. Patil, A. U. Borse, and K. J. Patil. The viscosity b and d coefficient (jonesdole equation) studies in aqueous solutions of alkyltrimethylammonium bromides at 298.15 k. *Journal of Molecular Liquids*, 200:416–424, 2014.

J. S. Patton and P. R. Byron. Inhaling medicines: delivering drugs to the body through the lungs. *Nature Reviews*, 6:67–74, 2007.

K. Perez-Toralla, J. Champ, et al. New non-covalent strategies for stable surface treatment of thermoplastic chips. *Lab on a Chip*, 13:4409–4418, 2013.

FASTCAM-APX RS Hardware Manual. Photron, 2006.

Z. Stojek. The electrical double layer and its structure. In F. Scholz, editor, *Electroanalytical Methods*. Springer, Berlin, Heidelberg, 2005.

A. Verschueren. Private communications. 2017.

H. Wijshoff. The dynamics of the piezo inkjet printhead operation. *Physics Reports*, 491:77–177, 2010.

Appendix A

Derivations and Computations

A.1 Hydrodynamic and electrokinetic properties

A.1.1 Viscosity

$$\eta/\eta_0 = 1 + A\sqrt{c} \tag{A.1}$$

$$A = 0.7536 \left[\frac{\lambda_1^0 + \lambda_2^0}{4\lambda_1^0\lambda_2^0} - \frac{\left(\lambda_1^0 - \lambda_2^0\right)^2}{4.41\lambda_1^0\lambda_2^0\left(\lambda_1^0 + \lambda_1^0\right)} \right] \tag{A.2}$$

Table A.1: The parameters with corresponding symbols, values and units, necessary to compute the change in viscosity between a 0.01 mM and a 1 mM sodium-chloride solution

Parameter	**Symbol**	**Value**	**Unit**
Viscosity pure solvent	η_0	0.0010016	Pa·s^{-1}
Electrolyte concentration	c	0.01	mM
		1	mM
Limiting equivalent conductance ion 1	λ_1^0	50.0852	μS· cm^{-1}
Limiting equivalent conductance ion 2	λ_1^0	76.3122	μS· cm^{-1}

The change in the viscosity between a solution with 0.01 mM sodium-chloride and a solution with 1 mM sodium-chloride is an increase of 0.5385 %.

A.1.2 Surface tension

$$\gamma = \gamma_0 + \frac{1}{2}z^2\lambda_B c k_B T \left[\ln\left(\frac{2}{\kappa\lambda_B}\right) - 2\gamma_E + \frac{3}{2} \right] \tag{A.3}$$

$$\kappa = \left(\frac{2cz^2e^2}{\varepsilon_r\varepsilon_0 k_B T} \right)^{1/2} \tag{A.4}$$

$$\lambda_B = \frac{e^2}{4\pi\varepsilon_r\varepsilon_0 k_B T} \tag{A.5}$$

Table A.2: The parameters with corresponding symbols, values and units, necessary to compute the change in surface tension between a 0.01 mM and a 1 mM sodium-chloride solution

Parameter	**Symbol**	**Value**	**Unit**
Surface tension pure solvent	γ_0	0.072	$N \cdot m^{-1}$
Electrolyte concentration	c	0.01	mM
		1	mM
Electrolyte valence	z	1	[-]
Boltzmann constant	k_B	$1.38064852 \cdot 10^{-23}$	m^2 kg/s^2/K
Temperature	T	293.15	K
Euler-Mascheroni constant	γ_E	0.57722	[-]
Elementary charge	e	$1.602177 \cdot 10^{-19}$	C
Relative dielectric constant of the solvent	ε_r	80.1	F/m
Vacuum permittivity	ε_0	$8.854188 \cdot 10^{-12}$	F/m

The change in the surface tension between a solution with 0.01 mM sodium-chloride and a solution with 1 mM sodium-chloride is an increase of 0.0246 %.

A.1.3 Density

$$\rho = \frac{\sum_{i=1}^{ion} x_i M_i + x_{H_2O} M_{H_2O}}{V_m} \tag{A.6}$$

$$V_m = \sum_{i}^{ion} x_i V_i + x_{H_2O} V_{H_2O}^{\Phi} \tag{A.7}$$

Table A.3: The parameters with corresponding symbols, values and units, necessary to compute the change in density between a 0.01 mM and a 1 mM sodium-chloride solution

Parameter	**Symbol**	**Value**	**Unit**
Molar fraction NaCl at 0.01 mM	x_i	$1.8051 \cdot 10^{-5}$	[-]
Molar fraction NaCl at 1 mM	x_i	$1.8051 \cdot 10^{-7}$	[-]
Molar mass of NaCl	M_i	58.44	g/mol
Molar fraction of water	x_{H_2O}	1	[-]
Molar mass of water	M_{H_2O}	18.015	g/mol
Molar volume of NaCl at 0.01 mM	V_i	$2.7056 \cdot 10^{-10}$	L/mol
Molar volume of NaCl at 1 mM	V_i	$2.7056 \cdot 10^{-8}$	L/mol
Molar volume of water	$V_{H_2O}^{\Phi}$	$1 \cdot 10^{-3}$	L/mol

The change in the density between a solution with 0.01 mM sodium-chloride and a solution with 1 mM sodium-chloride is an increase of 0.0058 %.

A.1.4 Electrical conductivity

$$\sigma = c\Lambda_{eq} \tag{A.8}$$

$$\Lambda_{eq} = ({\Lambda^0}_{eq,+} + {\Lambda^0}_{eq,-}) - \left(\frac{z^3 e^3 N_A}{3\pi\eta} \sqrt{\frac{2N_A}{\varepsilon k_B T}} + ({\Lambda^0}_{eq,+} + {\Lambda^0}_{eq,-}) \frac{z^3 e^3}{24\pi\varepsilon k_B T \left(1 + \sqrt{\frac{1}{2}}\right)} \sqrt{\frac{2N_A}{\varepsilon k_B T}} \right) \sqrt{c} \tag{A.9}$$

Table A.4: The parameters with corresponding symbols, values and units, necessary to compute the change in electrical conductivity between a 0.01 mM and a 1 mM sodium-chloride solution

Parameter	**Symbol**	**Value**	**Unit**
Electrolyte concentration	c	0.01	mM
		1	mM
Equivalent conductivity at infinite dilution positive ion	${\Lambda^0}_{eq,+}$	50.0852	μS$\cdot$ cm^{-1}
Equivalent conductivity at infinite dilution positive ion	${\Lambda^0}_{eq,-}$	76.3122	μS$\cdot$ cm^{-1}
Avogadro constant	N_A	$6.022{\cdot}10^{23}$	mol^{-1}
Viscosity of pure solvent	η	0.0010016	Pa$\cdot$s^{-1}
Electrical permittivity of water	ε	$6.906{\cdot}10^{-10}$	F/m

The electrical conductivity of a 1 mM sodium-chloride solution is 9.8 times higher than a 0.01 mM sodium-chloride solution.

A.2 Hagen-Poiseuille flow

This derivation of the velocity profile for a pressure driven flow through a tube with a circular cross section is based on the derivation of Kirby (2013). The following assumptions are made for this derivation:

1. All the flow moves in the z direction, so it is a unidirectional flow
2. The velocity gradients in the θ and z direction are zero
3. It is a steady flow
4. Convection can be neglected
5. The change in pressure in the z direction is uniform

A sketch of the final velocity profile of a flow through a circular tube can be found in Figure A.1.

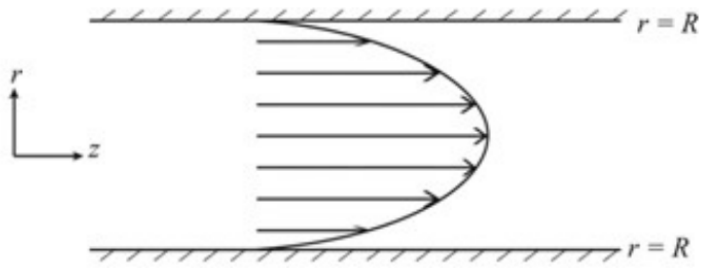

Figure A.1: Poiseuille flow in a circular tube with radius R (Beck-Broichsitter et al., 2014)

Starting from the Navier-Stokes equation:

$$\rho\frac{\partial\vec{\mathbf{u}}}{\partial t}+\rho\vec{\mathbf{u}}\cdot\nabla\vec{\mathbf{u}}=-\nabla p+\eta\nabla^2\vec{\mathbf{u}} \tag{A.10}$$

where ρ is the density of the fluid, $\vec{u}$ is the velocity in the x, y and z direction, t is the time, p is the pressure applied on the fluid and η is the viscosity of the fluid.

Using assumptions 3 and 4, so assuming the convection and unteady terms are zero, simplifies the equation to:

$$\nabla p=\eta\nabla^2\vec{\mathbf{u}} \tag{A.11}$$

For a radially symmetric flow, so using assumption 1, leads to:

$$\frac{\partial p}{\partial z} = \eta \frac{1}{r} \frac{\partial}{\partial r} r \frac{\partial u_z}{\partial r} \tag{A.12}$$

Using assumption 5, the pressure gradiant in the z-direction is uniform, and integrating w.r.t. r gives:

$$\frac{\partial p}{\partial z} \frac{r}{2\eta} + \frac{C_1}{\eta r} = \frac{\partial u_z}{\partial r} \tag{A.13}$$

Rearranging and integrating again w.r.t. r gives:

$$u_z = \frac{\partial p}{\partial z} \frac{r^2}{4\eta} + \frac{C_1}{\eta} \ln r + C_2 \tag{A.14}$$

The boundary condition are used to determine the integration constants. The boundary conditions are that the velocity of the flow is zero at the wall, so $u_z = 0$ at r=R, and that the velocity is at its maximum in the middle of the channel, so $\frac{\partial u_z}{\partial r} = 0$ at r=0. This gives a final velocity profile of:

$$u_z = -\frac{1}{4\eta} \frac{\partial p}{\partial z} \left(R^2 - r^2\right) \tag{A.15}$$

Appendix B

Supplementary Figures

B.1 Nebulizing with rotated configuration

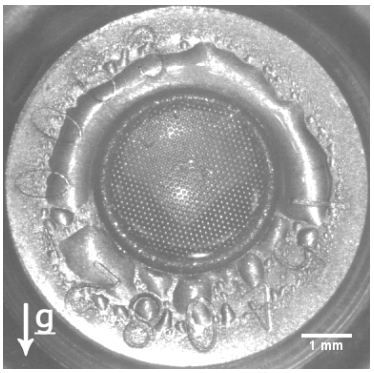

Figure B.1: Nebulization of DI water, a macroscopic view at t=2.58 s, with the nebulizer rotated 90 ° counterclockwise

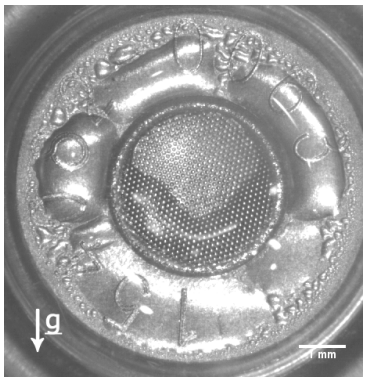

Figure B.2: Nebulization of DI water, a macroscopic view at t=2.58 s

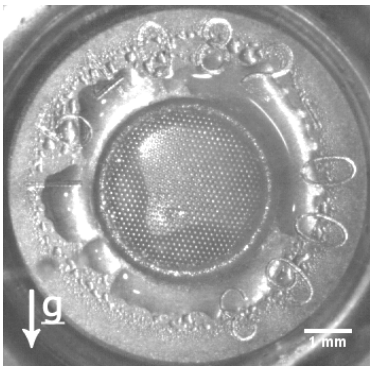

Figure B.3: Nebulization of DI water, a macroscopic view at t=2.58 s, with the nebulizer rotated 90 ° clockwise

B.2 Series of periods for different solutions

0.01 mM sodium-chloride

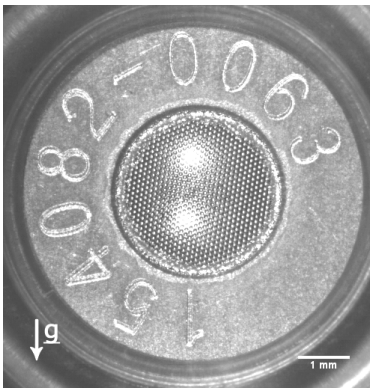

Figure B.4: Nebulization of a 0.01 mM sodium-chloride solution, a macroscopic view at t=0 s

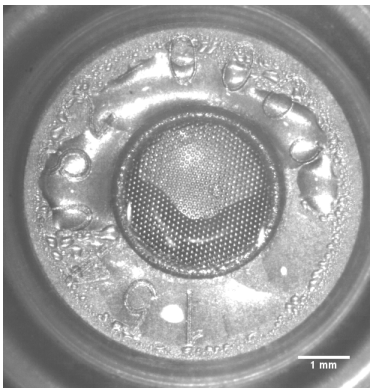

Figure B.5: Nebulization of a 0.01 mM sodium-chloride solution, a macroscopic view at t=3.74 s

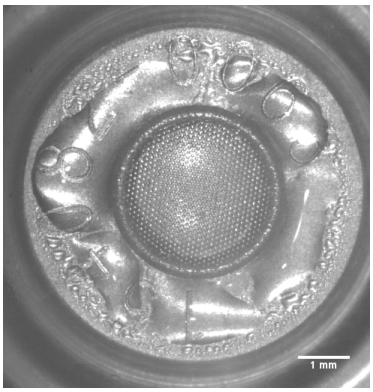

Figure B.6: Nebulization of a 0.01 mM sodium-chloride solution, a macroscopic view at t=5.81 s

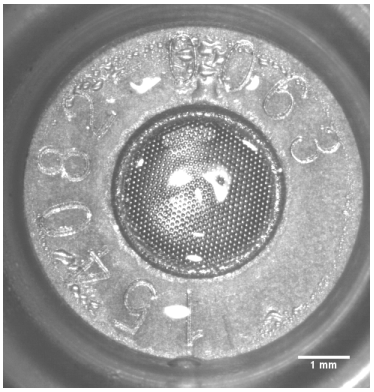

Figure B.7: Nebulization of a 0.01 mM sodium-chloride solution, a macroscopic view at t=6.74 s

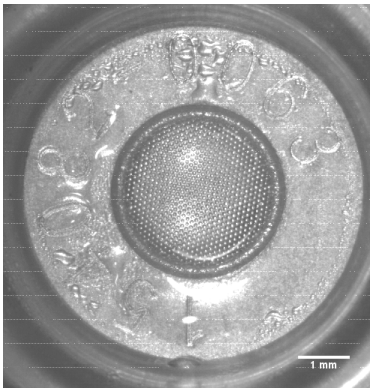

Figure B.8: Nebulization of a 0.01 mM sodium-chloride solution, a macroscopic view at t=7.67 s

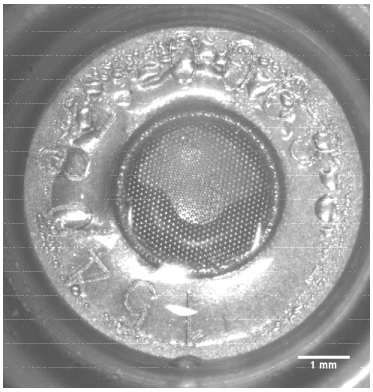

Figure B.9: Nebulization of a 0.01 mM sodium-chloride solution, a macroscopic view at t=9.88 s

0.05 mM sodium-chloride

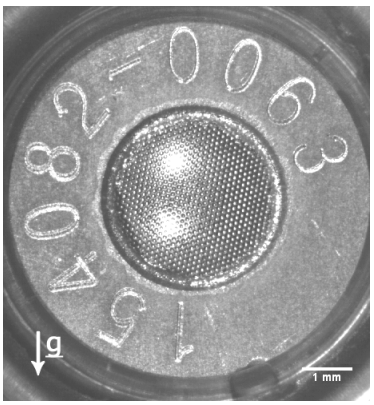

Figure B.10: Nebulization of a 0.05 mM sodium-chloride solution, a macroscopic view at t=0 s

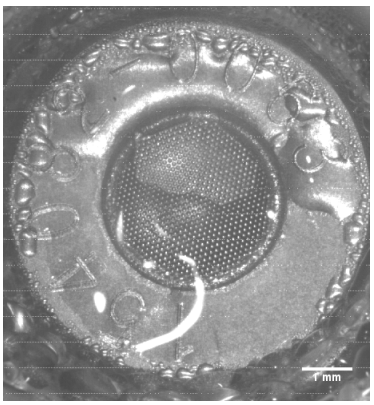

Figure B.11: NNebulization of a 0.05 mM sodium-chloride solution, a macroscopic view at t=8.052 s

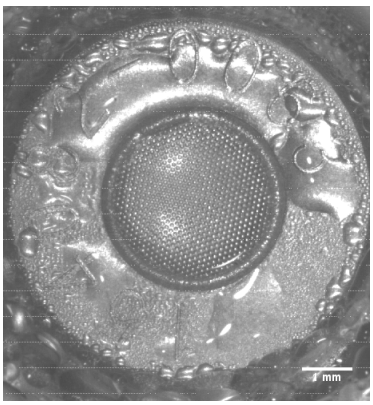

Figure B.12: NNebulization of a 0.05 mM sodium-chloride solution, a macroscopic view at t=9.135 s

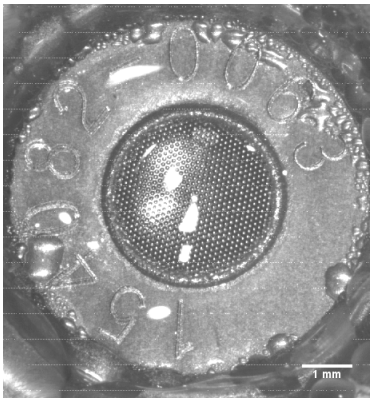

Figure B.13: Nebulization of a 0.05 mM sodium-chloride solution, a macroscopic view at t=19.99 s

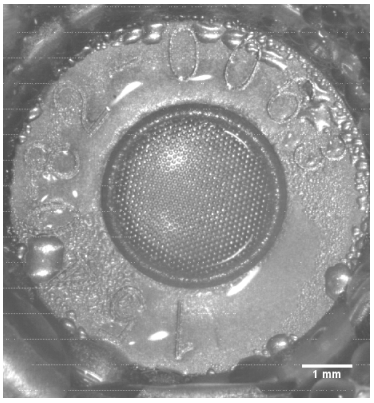

Figure B.14: Nebulization of a 0.05 mM sodium-chloride solution, a macroscopic view at t=21.379 s